

Carbon and nutrient accumulation in tropical mangrove creeks, Amazon region



Christiene R.L. Matos^{a,*}, José F. Berrêdo^{b,*}, Wilson Machado^c, Christian J. Sanders^d,
Edouard Metzger^e, Marcelo C.L. Cohen^a

^a Programa de Pós-Graduação em Geologia e Geoquímica, Universidade Federal do Pará, Belém, Pará, Brazil

^b Museu Paraense Emílio Goeldi/MCTIC, Belém, Pará, Brazil

^c Programa de Pós-Graduação em Geoquímica, Universidade Federal Fluminense, Niterói, Rio de Janeiro, Brazil

^d National Marine Science Centre, Southern Cross University, Coffs Harbour, New South Wales, Australia

^e Laboratoire des Bio-Indicateurs Actuels et Fossiles, UMR6112 CNRS LPG-BIAF, Université d'Angers, Angers, France

ARTICLE INFO

Keywords:

Blue carbon
Organic matter source
Macrotidal estuary
Creek mudflat
Brazilian Amazon coast

ABSTRACT

The Marapanim River estuary (MRE) is part of the Amazon estuarine system located in northern Brazil, which is characterized as having extensive mangrove forests. Given that previous studies reported CO₂ and CH₄ fluxes from mangrove creeks in this region, here we investigate the potential organic carbon sequestration of the creek mudflats to get a better understanding of the carbon cycling through these systems. Sediment accumulation rates derived from ²¹⁰Pb dating indicated that sampled cores represent the previous 24 (± 4) yr. The approximately 24-year total organic carbon (TOC), total nitrogen (TN) and total phosphorus (TP) burial rates were estimated to be 192.5 (± 43.5), 15.3 (± 4.1) and 3.2 (± 0.8) g m⁻² yr⁻¹, respectively. A binary source mixing model based on carbon stable isotopes (δ¹³C) revealed that the sedimentary organic matter (OM) is mainly influenced by marine phytoplankton input (49% to 95%). Furthermore, the TOC accumulation rates found here were slightly higher than the global averages estimated for within mangrove forests, suggesting that these unaccounted carbon sinks along creek mudflat environments are relevant for carbon budgets in mangrove-colonized coastal zones. The highest contents, stocks and accumulation rates were found in the tidal creek sediments that are most influenced by nearby mangroves and are more protected than sediments from major river margins. Our results indicate that the creek mudflats play a major role in carbon and nutrients sequestration, directly related to grain size and OM sources.

1. Introduction

Mangrove forests, along with other vegetated coastal ecosystems such as seagrasses and saltmarshes, are recognized as blue carbon ecosystems due to their capacity to sequester carbon at a far higher rate than terrestrial forests (Nellemann et al., 2009; Mcleod et al., 2011). Although mangrove forests occupy < 1% of the global coastal area, these ecosystems sequester and store high amounts of organic carbon in plant biomass and sediment, contributing 10–15% to coastal sediment carbon storage and exporting 10–11% of the particulate terrestrial carbon to the ocean (Jennerjahn and Ittekkot, 2002; Dittmar et al., 2006; Alongi, 2014). For instance, the carbon stocks in the Amazon mangroves are over twice those of upland evergreen forests and almost 10-fold those of tropical dry forests (Kauffman et al., 2018), which

underscores their potential value to mitigating greenhouse gas emissions.

Two important measurements used in determining the rate of organic carbon sequestration are the sediment total organic carbon (TOC) content and the sediment accumulation rate (SAR). The first term provides information about the TOC stock sequestered in sediments (Howard et al., 2014). The SAR is used to measure the TOC accumulation rates, which address the question of how much TOC is sequestered in a specified period and quantifies the ongoing sink capacity (Arias-Ortiz et al., 2018; Wang et al., 2019). From the ²³⁸U decay series, the ²¹⁰Pb dating method has been an ideal tracer for dating aquatic sediments deposited during the previous 100 years, enabling the determination of TOC accumulation rates in vegetated coastal ecosystems (Smoak et al., 2013; Marchio et al., 2016; Sanders et al., 2016; Sasmito

* Corresponding authors at: Museu Paraense Emílio Goeldi, Av. Perimetral, 1901 – CEP, 66077-830 Belém, Pará, Brazil.

E-mail addresses: christienematos@hotmail.com (C.R.L. Matos), berredo@museu-goeldi.br (J.F. Berrêdo), wmachado@geoq.uff.br (W. Machado), christian.sanders@scu.edu.au (C.J. Sanders), edouard.metzger@univ-angers.fr (E. Metzger), mcohen80@hotmail.com (M.C.L. Cohen).

<https://doi.org/10.1016/j.margeo.2020.106317>

Received 10 January 2020; Received in revised form 10 August 2020; Accepted 12 August 2020

Available online 15 August 2020

0025-3227/ © 2020 Elsevier B.V. All rights reserved.

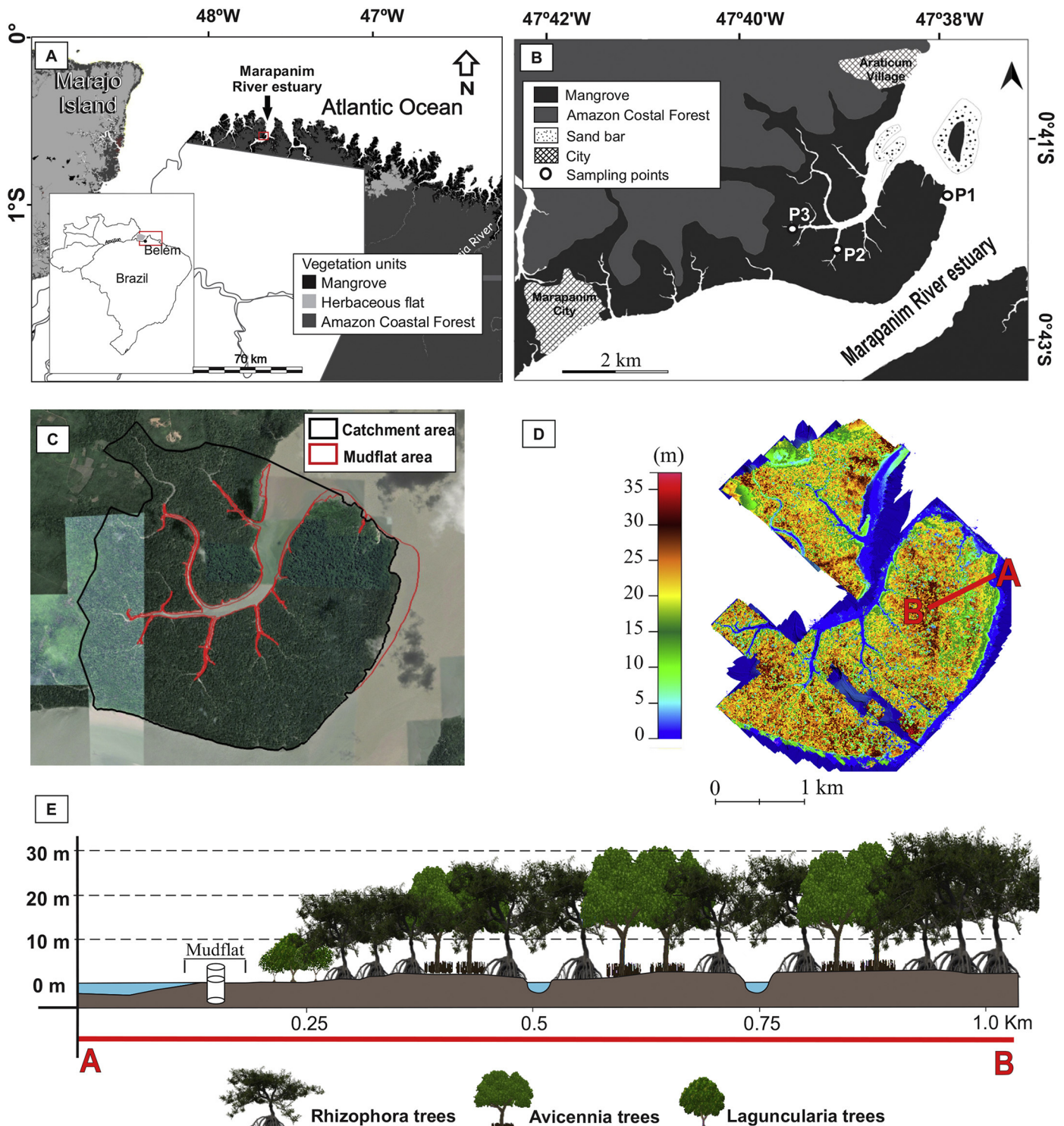


Fig. 1. (A) and (B) Map of the study area in Marapanim estuarine mangrove, Brazil. (B) Sampling location (P1, P2 and P3). (C) Catchment and mudflat areas related to the sampling sites. (D) Digital vegetation height model. (E) The diagrammatic mangrove forest distribution and positioning of the sampled cores in the mud tidal flat mangrove sediments. Black dashed lines represent the height of the mangrove.

et al., 2020).

Total organic carbon to total nitrogen ratios TOC/TN ratios, and carbon and nitrogen stable isotope signatures ($\delta^{13}\text{C}$ and $\delta^{15}\text{N}$) have been widely used as effective geochemical proxies to estimate the relative proportions of terrigenous and marine OM in estuarine and coastal sediments (Lamb et al., 2006; Ranjan et al., 2011; Liu et al., 2015; Vilhena et al., 2018; Kusumaningtyasa et al., 2019). Previous studies have shown that the terrestrial OM is preserved, stored and

accumulates more efficiently than marine-derived OM in sediments (Hedges et al., 1997; Ranjan et al., 2011; Watanabe and Kuwae, 2015; Kusumaningtyasa et al., 2019), due to the selective preservation of refractory OM at the expense of labile components, which is more susceptible to degradation by microorganisms (Hedges et al., 1997; Zonneveld et al., 2010). Therefore, identifying the source of OM is important in evaluating the effectiveness of the mangrove ecosystems as blue carbon sinks, since the variability of the origin of the OM stored

in sediments contributes differently to longer-term carbon burial.

Data on the contribution of intertidal creek environments are more limited than mangrove forests as carbon sinks. However, intertidal mudflats situated along mangrove creeks can play an important role in the carbon cycling of tropical land-sea interfaces, such as acting as a conduit for exchanges between mangrove forests and coastal waters. For instance, Call et al. (2019) demonstrated that a mangrove tidal creek in the Amazon region presented large CO₂ and CH₄ fluxes, suggesting that recent global estimates of these fluxes, based mostly on data from higher latitudes (exceeding 5°) without considering macrotidal mangrove system, may be underestimated. Moreover, tidal creeks may be more sensitive to land-use changes than open water systems due to a broader connectivity with watersheds, implying that OC accumulation rate changes by up to one order of magnitude in response to urban effluents input (Darrow et al., 2017). Therefore, the balance between carbon export, and sediment burial may present an important conduit to the mangrove and coastal ocean carbon cycle.

The Brazilian coastal region holds, over 960,000 ha, the third-largest mangrove area worldwide (Giri et al., 2011) including the North coast of Brazil (known as the Brazilian Amazon coast) which is considered the largest continuous and best-preserved mangrove forest in the world (Nascimento et al., 2013; Kauffman et al., 2018). The mangroves of the Marapanim River estuary (MRE) are part of this extensive range of mangroves on the Brazilian north coast, which present minimal anthropogenic impact. Mangroves are enormously important in this region as they sustain traditional communities found on the Amazon coast (Fernandes et al., 2018). Information on the biogeochemical cycling of carbon and nutrients in a non-impacted environment is necessary to better understand how potential changes to the mangrove dynamics may impact the carbon and nutrient fluxes between mangrove forests and coastal waters.

The main goal of this study is to obtain a better understanding of the cycling of sedimentary OM in the Marapanim mangrove estuarine system, located in the Brazilian Amazon region. To this aim, the hypothesis that creek mudflats play an important role as carbon and nutrient sinks, rather than only act as a conduit for carbon and nutrients cycling in coastal regions, was tested. We analyzed TOC, TN and TP stocks (sediment) and accumulation rates, as well as estimated the sources of OM in unvegetated mudflats situated along mangrove creeks to: 1) characterize the different OM sources, and 2) investigate potential relationships between OM sources and TOC, TN, and TP burial based on accumulation rates. In addition, we characterized the mangrove forest, according to topographical gradients of the tidal flats and vegetation heights, since biogeochemical cycles and carbon budgets are also affected by the mangrove structure and environmental conditions (Chambers et al., 2013; Pérez et al., 2018; Steinmuller et al., 2020). As such, we suggest that mangrove characteristics should be considered when comparing the biogeochemical data obtained here with other studies.

2. Materials and methods

2.1. Study area

The Marapanim River estuary is part of the Amazon estuarine system in Para, Northern Brazil, between 00°30' to 01°00'S and 47°32' to 47°00'W (Fig. 1a). The main River channel has a funnel form, with a length of more than 70 km and a width of 8 km at the mouth (Atlantic Ocean) (Silva et al., 2009). The water in the estuary is extremely mixed as a result of tidal pumping and wave action, with the ocean water penetrating approximately 62 km up the estuary mouth during the dry season and 42 km during the wet season (Berrêdo et al., 2008). This system is dominated by a macrotidal regime with semidiurnal tides; with an amplitude range from 3.5 m during neap tide to over 6 m during spring tides.

The coastal region of Para is characterized by a tropical climate,

with a wet season from January to June, and a dry season from July to December, high annual precipitation (2500–3000 mm) and average annual temperature of 27.7 °C (Martorano et al., 1993). The water temperature of the estuary varies from 27 to 30 °C. pH values indicate alkaline conditions during the dry season (7.9 to 8.0) and slightly acidic during wet season (5.7 to 6.7). The salinity at low and high fluvial discharge varies from 24 to 3, respectively, along the estuarine channel (Berrêdo et al., 2008).

The estuary is part of the Master Lucindo Marine Extractivist Reserve, a protected Conservation Unit region. The estuary contains 130 km² of continuous and pristine mangrove forest (Vilhena et al., 2013). The dominant mangrove species are *Rhizophora* spp., *Avicennia germinans*, and *Laguncularia racemosa*. The trees are tall (up to approximately 35 m, Fig. 1d), generally distributed in mixed forests of *Rhizophora* spp. and *Avicennia germinans*. *Laguncularia racemosa* is found in the mangrove fringe. Saltmarsh vegetation is represented by *Spartina brasiliensis*, which occupies a pioneering position along mudflat accretion areas.

The Marapanim catchment extends over an area of 2500 km² (Silva et al., 2009), with no industrial development, where about 28,000 people live. Like other Brazilian Amazon coastal cities, the Marapanim city's economy is based mainly on the sustainable use of natural resources, particularly fishing (crabs, shrimps, mollusks and fish), as well as commerce and tourism (Kjerve and Lacerda, 1993; ICMBio, 2018; Fernandes et al., 2018).

2.2. Acquisition of drone images and processing

Very high resolution (3 cm) images of the study area were obtained using a Drone Phantom 4 DJI (FC 330 digital 4 K/12MP camera). The planialtimetric data were processed by the Agisoft Photoscan version 1.6.1 (AgisoftPhotoScan, 2018), and Global Mapper version 19 (GlobalMapper, 2017). Planialtimetric data of ten ground control points were acquired by a smartphone connected to an Antenna Trimble Catalyst with a differential Global Navigation Satellite System (GNSS). A sub-metric correction (± 30 cm), provided by the Trimble website upon payment of a subscription (<https://geospatial.trimble.com/catalyst-subscriptions>), was applied to the GNSS data. The vegetation was manually classified by photointerpretation in the Global Mapper Software. *Rhizophora*, *Avicennia*, and *Laguncularia* trees were identified according to color, geometry, and texture of the canopy. This work followed procedures described by the software developer (AgisoftPhotoScan, 2018; “Global Mapper User's Manual,” 2020) and adapted for mangrove areas (Cohen et al., 2018, 2019). A detailed description of the data processing can be obtained in the supplementary information section.

2.3. Field sampling

The sediment core collection was conducted during the wet (May 2017) and dry (Sept 2017) seasons. The sampling sites were situated near the mouth (Atlantic Ocean) of the MRE, along a lobular structure, where mangrove vegetation has developed. We compared tidal mangrove creeks (P2 and P3) with the Marapanim River margin (P1), which is located in an area under the influence of a nearby sand bar (Fig. 1b).

2.3.1. Sediment

One sediment core was collected from the unvegetated mudflat (devoid of macrophytes) at each site by inserting an acrylic tube (50 cm length) vertically into the substrate during low tide. Immediately after extraction, the sediment core was sectioned at 1-cm depth intervals from the core top to 6 cm depth, then 2-cm intervals until the 20 cm depth, finally at 5-cm intervals until the 35 cm depth. The sub-samples were bagged, preserved on ice and then transported to the laboratory. In addition, pore waters were retrieved using Rhyzon® collectors (Seeberg-Elverfeldt et al., 2005) at the same intervals to the solid phase

for salinity analysis. Pore water salinity was measured in situ with a portable refractometer (Atago).

2.3.2. Vegetation and phytoplankton

The phytoplankton and vegetation collection was conducted just during the wet (May 2017) season. Approximately 15 fresh leaves of six different adult trees of each dominant mangrove species (*Rhizophora* spp., *Avicennia germinans* and *Laguncularia racemosa*) were collected. The leaves were washed in deionized water to remove the adhered sedimentary particles and salt, then the samples were frozen and lyophilized. The phytoplankton samples were collected along the mangrove tidal creek during the flood tides ($n = 3$); horizontal hauls were performed on the water surface (maximal depth 50 cm), using a standard-type plankton mesh, with mesh opening 64 μm . This mesh opening is the most used one in the Amazon estuaries due to the strong local hydrodynamics (Paiva et al., 2006). Each sample was observed in a binocular microscope after it was washed in deionized water and subjected to wet sieving (mesh opening 20 μm) to remove the contaminant particles (leaves and shells) or possible zooplankton predators. Finally, the samples were frozen and lyophilized.

2.4. Analyses and data treatment

2.4.1. DBD and grain size

Dry bulk density (DBD, g cm^{-3}) was determined as the dry sediment weight (g) divided by the initial volume (cm^3). From the original wet section, a portion was taken for grain size analysis. The sediment grain size was determined using a Fritsch particle size meter model Analysette 22, after calcium carbonate and OM removal, and dispersion in sodium hexametaphosphate 4% (Loring and Rantala, 1992). The GRADISTAT 9.1 software (Blott and Pye, 2001) was used for treating results, where the grain size scale was modified from Udden (1914) and Wentworth (1922), with the classification of clay (< 2 μm), silt (2–63 μm) and sand (> 63 μm) are established for these fractions.

2.4.2. Elemental and stable isotope analysis

Carbon and nitrogen stable isotope ratios of phytoplankton, leaves and sediments were measured to identify the sources of OM contributing to the sediments column at each site. A subsample of each core fraction was acidified to remove carbonate material; then it was washed in deionized water, dried (60 °C) and ground to powder before TOC and $\delta^{13}\text{C}$ analyses. TN and $\delta^{15}\text{N}$ were analyzed in non-acidified subsamples. Isotopic signatures ($\delta^{13}\text{C}$ and $\delta^{15}\text{N}$) and TOC and TN contents were analyzed using a Leco Flash Elemental Analyzer coupled to a Thermo Fisher Delta V isotope ratio mass spectrometer (Thermo Flash EA 1112) (Carvalho et al., 2020). Analytical precision was as follows: TOC = 0.1%, TN = 0.1%, $\delta^{13}\text{C}$ = 0.1‰, and $\delta^{15}\text{N}$ = 0.15‰. Working standards were used (glucose, 10.7 ppt and urea, 41.3 ppt) to calibrate for $\delta^{13}\text{C}$. A pair of standards were measured with every 20 samples. These standards were calibrated initially against international absolute standards LSVEC and NIST8542. TP contents in the sediments were determined by colorimetry, according to Grasshoff et al. (1999), following the extraction procedure from Aspila et al. (1976). The results of TOC, TN and TP, expressed in % in this work, were converted to $\mu\text{mol g}^{-1}$ dry weight sediment to calculate individual TOC/TN/TP molar ratios.

2.4.3. Calculation of marine and terrestrial organic matter

The relative proportions of mangrove/terrestrial OM (OM_{terr}) and marine OM (OM_{mar}) in sediment cores were estimated using the two end-member mixing model described in Schultz and Calder (1976):

$$F_{\text{terr}} = (\delta^{13}\text{C}_{\text{mar}} - \delta^{13}\text{C}_{\text{sed}}) / (\delta^{13}\text{C}_{\text{mar}} - \delta^{13}\text{C}_{\text{terr}}) \times 100 \text{ and } F_{\text{mar}} = 100 - F_{\text{terr}} \quad (1)$$

where F_{terr} is the contribution from the mangrove/terrestrial fraction, F_{mar} is the contribution from the marine fraction, $\delta^{13}\text{C}_{\text{sed}}$ value of the

sediment interval, and $\delta^{13}\text{C}_{\text{terr}}$ and $\delta^{13}\text{C}_{\text{mar}}$ are the terrestrial and marine end-members value, respectively. We estimated the terrestrial (an average of the plants that dominate in the Marapanim mangrove) and marine (phytoplankton-derived OM) end-member $\delta^{13}\text{C}$ values to be $-29.9 \pm 1.0\text{‰}$ ($n = 18$) and $-23.9 \pm 0.7\text{‰}$ ($n = 3$), respectively, from our results.

2.4.4. ^{210}Pb dating and rates of organic carbon, nitrogen and phosphorus accumulation

To date sediments, we measured radionuclide activities from the ^{238}U decay series in a high-purity germanium (HPGe) well gamma detector with 40% efficiency coupled to a multichannel analyzer. Sediments at each interval were sealed in gamma tubes for at least three weeks to establish secular equilibrium between ^{226}Ra and its daughter products ^{214}Pb and ^{214}Bi . The ^{210}Pb activities were determined by the direct measurement of 46.5 KeV gamma peaks, while ^{226}Ra activity was calculated averaging its daughters' peaks ^{214}Pb and ^{214}Bi (295.2 KeV) (351.9 KeV) (609.3 KeV) (Sanders et al., 2016). The excess ^{210}Pb ($^{210}\text{Pb}_{\text{ex}}$) activity was estimated by subtracting the ^{226}Ra from the total ^{210}Pb activity. The sediment accumulation rate (SAR) was calculated according to the Constant Initial Concentration (CIC) method as a net downcore decrease in $^{210}\text{Pb}_{\text{ex}}$ activities was noted in all three cores, implying a consistent rate of sedimentation (Appleby and Oldfield, 1992). Accumulation rates and stocks (for 0–35 cm) of TOC, TN and TP were estimated for each depth interval (cm), using values of SAR (cm yr^{-1}), DBD (g cm^{-3}), and TOC, TN as well as TP contents (g g^{-1}), respectively:

Accumulation rates (AR) ($\text{g m}^{-2} \text{yr}^{-1}$) = [SAR] x [DBD] x [TOC, TN or TP content] (2).

Stocks (g m^{-2}) = [DBD] x [depth] x [TOC, TN or TP content] (3).

2.4.5. Statistical analysis

Statistical analyses were performed using statistical package PAST version 3.26 (Hammer et al., 2001). One-way analysis of variance (ANOVA) was used to assess the significant difference of a single variable (clay, silt, sand, TOC, TN, TP, $\delta^{13}\text{C}$, $\delta^{15}\text{N}$) between the sampling sites (P1, P2 and P3) and seasons (wet and dry), with a Tukey HSD post hoc test for distinguishing pairwise relationships among sites. The normality of data distribution was tested using Shapiro-Wilk prior to statistical analysis. When the variables were not normally distributed (clay, silt, sand, TOC, TN and TP), they were log-transformed to fit a normal distribution. Statistical significance at $\alpha < 0.05$ was used for all tests. Principal Components Analysis (PCA) was applied to identify the multivariate relationships between the geochemical variables. Significant factors were selected based on eigenvalues > 1. The relation between each pair of variables was measured by Pearson's correlation coefficient. Correlation coefficients greater than 0.5 were considered significant.

3. Results

3.1. Mangrove structure

The A-B profile (Fig. 1d-e) revealed a young mangrove fringe (1–10 m) mainly represented by *Laguncularia racemosa* in the topographically lowest sector (~1 m above mean sea-level, amsl) of the tidal flat. In an intermediate topography (1–2 m amsl) a dense mangrove forest characterized by *Laguncularia racemosa* and *Rhizophora* spp. (10–20 m tall) was found. Following the topographical gradient (~2 m amsl) a mixed forest of *Avicennia germinans* and *Rhizophora* spp. is noted (20–30 m tall). These trees become taller (25–33 m) in the inner parts of this mangrove forest. The sampling sites P2 and P3 (Fig. 1b) were located in topographically highest areas, inundated only during spring tides, of which sediments are strongly oxidized during the dry season, coexisting with more mature mangroves (15–25 m).

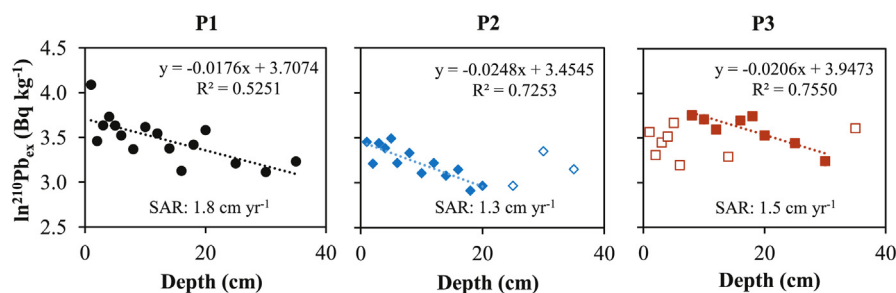


Fig. 2. $\ln^{210}\text{Pb}_{\text{ex}}$ (Bq kg^{-1}) activities versus depth in the sediment cores (P1, P2 and P3), sedimentation rates were calculated using selected points of $^{210}\text{Pb}_{\text{ex}}$ profiles (filled symbols). Open symbols correspond to result interpreted as biologically and physically disturbed.

3.2. Sediment chronology

The $\log^{210}\text{Pb}_{\text{ex}}$ of the sedimentary profiles from the three examined sampling sites were depicted by an almost linear decline with depth (Fig. 2), implying a consistent rate of sedimentation. Based on the $^{210}\text{Pb}_{\text{ex}}$ profiles, the top 6 cm of the P3 and bottom of the P2 sediment cores were determined to be mixed and therefore, were excluded when calculating SAR. The SAR were calculated as 1.8 (core P1), 1.5 (core P3) and 1.3 (core P2) cm yr^{-1} , respectively (Fig. 2), with a regional mean of $1.5 \pm 0.3 \text{ cm yr}^{-1}$. According to the extrapolated $^{210}\text{Pb}_{\text{ex}}$ -derived age, sediment at the core basis corresponds to an age of about 1997 year in P1 (35 cm), 1989 year in P2 (35 cm) and 1994 in P3 (35 cm).

3.3. Grain size and dry bulk density

The textural composition of the sediments was mostly sand and silt (34–80% of silt, 12–64% of sand) with a low percentage of clay (< 10%) (Fig. 3). This textural distribution differs among the three sites ($p < 0.05$, Table 2), with the distribution of fine-grained higher at sites P2 and P3 compared with P1 (Fig. 3). The contents of the grain size fractions also showed significant seasonal variations (Table 2), except to silt at P3 and sand at P1 and P2. In general, values of DBD (g cm^{-3}) in the sediment sites increased substantially with the depth (Fig. 3). The highest DBD was found in the P1, exceeding 1.0 g cm^{-3} , where the sedimentary profile graded to predominately sand.

3.4. Elemental and isotopic composition

The values and vertical profiles of elemental and isotopic composition for the sediments, plants and phytoplankton are shown in Table 1 and Fig. 3. Differences in TOC, TN, TP contents of sediments between sampling locations and seasons (except to TN at site P3) were statistically significant (Table 2). The range of TOC was highest at sites P2 (2.28 to 3.84%) and P3 (2.21 to 3.04%) compared to P1 (0.53 to 1.91%). The range of TN was similar to P2 (0.19 to 0.27%) and P3 (0.19 to 0.26%) compared to P1 (0.04 to 0.17%). Like TOC and TN, TP contents was much larger in the P2 (0.028 to 0.052%) and P3 (0.033 to 0.059%) than to P1 (0.009 to 0.044%). In all three sites, TOC, TN and TP contents decreased slightly with depth.

The $\delta^{13}\text{C}$ values of sediments varied from -26.9 to -24.2‰ , with significant difference between sites ($p < 0.05$). The downcore $\delta^{13}\text{C}$ profile was relatively homogeneous at site P1, without significant difference between seasons ($p > 0.05$), with an average of $-25.2 \pm 0.4\text{‰}$. However, P2 and P3 showed significant differences between seasons ($p < 0.05$), due to results from upper 18 cm, with highest values during dry season, with average of $-25.7 \pm 0.6\text{‰}$ and $-25.2 \pm 0.5\text{‰}$, compared to wet season, with average of $-26.6 \pm 0.2\text{‰}$ and $-26.3 \pm 0.2\text{‰}$, respectively.

The $\delta^{15}\text{N}$ values of sediments did not differ significantly between seasons ($p > 0.05$), but differed significantly between sites ($p < 0.05$). The $\delta^{15}\text{N}$ values ranged from 5.1 to 8.4‰, with an average

of $6.1 \pm 0.8\text{‰}$ to P1, $5.9 \pm 0.6\text{‰}$ to P2 and $6.5 \pm 0.3\text{‰}$ to P3. Downcore profiles of $\delta^{15}\text{N}$ showed a small increase with depth, excepted for site P1 that showed oscillations and no tendency with depth, with a peak at 14 cm.

Differences in TOC/TN molar ratios between sampling locations and seasons were statistically significant (Table 2), varying from 12 to 18.5, with an average of 15.3 ± 1.3 to P1, 15.6 ± 1.3 to P2 and 13.7 ± 0.8 to P3. Downcore profiles of TOC/TN showed a small increase with the depth at all sites. The TN/TP molar ratios in sediments were not significantly different in terms of spatial variability ($p > 0.05$), but were significantly different seasonally, with highest ratios in the wet season, varying from 8.3 to 13.3, compared to dry season, that varied from 2.9 to 11.8.

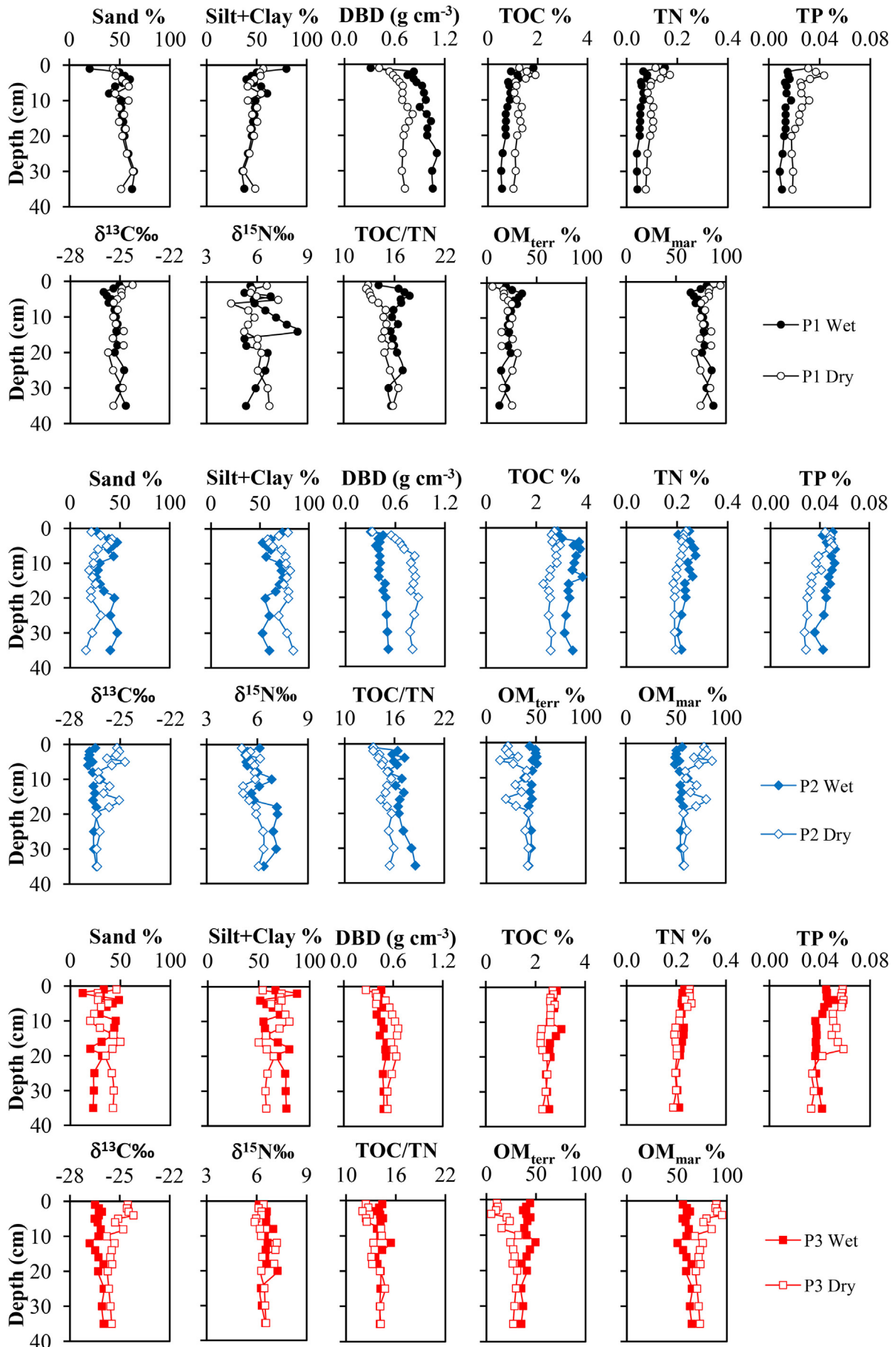
The $\delta^{13}\text{C}$ values of *Rhizophora* spp., *Avicennia germinans* and *Laguncularia racemosa* leaves were similar and ranged from -31.8 to -28.2‰ ($29.8 \pm 1.0\text{‰}$), which is within the range of C_3 terrestrial plants. The $\delta^{15}\text{N}$ and TOC/TN values varied slightly from species to species from 1.7 to 6.4‰ ($4.4 \pm 1.3\text{‰}$) and from 30.0 to 40.1 (34.0 ± 3.2), respectively. The phytoplankton presented $\delta^{13}\text{C}$ values from -24.4 to -23.4‰ ($23.9 \pm 0.7\text{‰}$), $\delta^{15}\text{N}$ from 3.2 to 3.7‰ ($3.4 \pm 0.4\text{‰}$), and TOC/TN from 6.9 to 7.2 (7.1 ± 0.2).

3.5. Principal Component Analysis (PCA)

The significant components (ie., eigenvalue > 1) loading matrix of PCA are listed in Table 3. The PCA (Fig. 4) showed that the first two components together explained 74.5% of the data variation. The first component (PC1) accounted for the largest proportion with 61.7% of the total variance. It showed significant positive loading (> 0.5) for TN, TOC, TP, silt and clay, and negative loading of sand and $\delta^{13}\text{C}$. The first component explained the variations between the sites, separating the site P1 from P2 and P3 due to its high sand content (Fig. 4a). This component also gives strong evidence of TOC, TN and TP increase with increase of silt and clay, with the highest TOC, TN and TP contents for P2 and P3 (Fig. 4b). The second component (PC2) explained 12.9% of the total variance and showed significant loading only for $\delta^{15}\text{N}$.

3.6. Proportions of organic matter sources

The proportions of terrestrial (OM_{terr}) and marine (OM_{mar}) OM sources were derived from the $\delta^{13}\text{C}$ data and Eq. (1). Downcore profiles of OM_{mar} and OM_{terr} remained relatively constant throughout the sediment columns during the wet season, but during the dry season an increase in marine input in the upper layers (< 18 cm) was observed at sites P2 and P3 (Fig. 3). Relatively high proportions of OM_{mar} were observed at all sites in both wet and dry seasons. Overall, OM_{mar} varied from 49.1 to 95.2% and OM_{terr} from 4.8 to 50.9% (Table 1). In the wet season, OM_{mar} contribution was highest in the site P1 (76.4%) compared to sites P2 (54.5%) and P3 (60%). During dry season, OM_{mar} increased to 79.6, 69 and 78% at sites P1, P2 and P3, respectively.



(caption on next page)

Fig. 3. Depth profiles of grain size, DBD, TOC, TN, TP, $\delta^{15}\text{N}$, $\delta^{13}\text{C}$ and TOC/TN (molar ratio) for the sediment cores (P1, P2 and P3). Including proportions of terrestrial (OM_{terr}) and marine (OM_{mar}) sedimentary OM, during wet (filled circles) and dry (open circles) seasons.

3.7. Stocks and accumulation rates

The TOC, TN and TP accumulation rates and stocks are shown in Fig. 5 and Table 4. The TOC, TN, and TP accumulation rates were estimated from SAR, DBD and TOC, TN and TP content results (Eq. (2)). The downcore sediment densities along with the TOC, TN and TP contents were used to determine stocks (Eq. (3)), the stocks were calculated to 30 cm sediment depth for the three sampling sites. The TOC, TN and TP accumulation rates showed significant site-difference ($p < 0.05$), with a regional mean of $192.5 \pm 50.6 \text{ g m}^{-2} \text{ yr}^{-1}$ for TOC, $15.3 \pm 4.3 \text{ g m}^{-2} \text{ yr}^{-1}$ for TP and 3.2 ± 1.0 for TP. The highest TOC, TN, and TP accumulation rates were measured at sites P2 (C: 218.7, N: 16.4, and P: $3.1 \text{ g m}^{-2} \text{ yr}^{-1}$) and P3 (C: 215.8, N: 18.4, and P: $3.9 \text{ g m}^{-2} \text{ yr}^{-1}$) and the lowest were measured at site P1 (C: 143.2, N: 11.0, and P: $2.7 \text{ g m}^{-2} \text{ yr}^{-1}$). The TOC, TN and TP stocks also differed significantly among the three sites ($p < 0.05$), with a regional mean of $3811 \pm 1389 \text{ g m}^{-2}$ for TOC, $296 \pm 109 \text{ g m}^{-2}$ for TN and $58 \pm 15 \text{ g m}^{-2}$ for TP. Similarly, the TOC, TN and TP stocks were higher at sites P2 (C: 5217.8, N: 386.3, P: 64.9 g m^{-2}) and P3 (C: 3878.6, N: 325.8, P: 55.4 g m^{-2}) than P1 (C: 2337.5, N: 177.1, P: 17.1 g m^{-2}).

Table 2

One-way ANOVA for different geochemical parameters in the sediment cores (P1, P2 and P3), during wet and dry seasons. Superscript lowercase letters indicate statistically equal means by the Tukey post hoc test.

Parameters	Between sites		Between seasons (p value)		
	(p value)	Tukey test	P1	P2	P3
TOC	< 0.05	P2 ^a P3 ^b P1 ^c	< 0.05	< 0.05	< 0.05
TN	< 0.05	P2 ^a P3 ^a P1 ^b	< 0.05	< 0.05	0.69
TP	< 0.05	P2 ^a P3 ^a P1 ^b	< 0.05	< 0.05	< 0.05
$\delta^{13}\text{C}$	< 0.05	P1 ^a P2 ^b P3 ^b	0.14	< 0.05	< 0.05
$\delta^{15}\text{N}$	< 0.05	P3 ^a P1 ^b P2 ^b	0.36	0.07	0.29
TOC/TN	< 0.05	P1 ^a P2 ^a P3 ^b	< 0.05	< 0.05	< 0.05
TN/TP	0.11	P1 ^a P2 ^a P3 ^a	< 0.05	< 0.05	< 0.05
Clay	< 0.05	P2 ^a P3 ^a P1 ^b	< 0.05	< 0.05	< 0.05
Silt	< 0.05	P2 ^a P3 ^a P1 ^b	< 0.05	< 0.05	0.51
Sand	< 0.05	P1 ^a P2 ^b P3 ^b	0.14	< 0.05	0.29
TOC AR	< 0.05	P3 ^a P2 ^b P1 ^c			
TN AR	< 0.05	P3 ^a P2 ^b P1 ^c			
TP AR	< 0.05	P3 ^a P2 ^b P1 ^c			
TOC Stocks	< 0.05	P2 ^a P3 ^{a,b} P1 ^b			
TN Stocks	< 0.05	P2 ^a P3 ^a P1 ^b			
TP Stocks	< 0.05	P2 ^a P3 ^a P1 ^b			

Table 1

Minimum, maximum, mean values and standard deviation (\pm SD) of TOC, TN and TP contents, TOC/TN and TN/TP molar ratios, and $\delta^{15}\text{N}$ and $\delta^{13}\text{C}$ for the sediment cores (P1, P2 and P3), plants (Avicennia (Avi.), Laguncularia (Lag.), Rhizophora (Rhi.)) and phytoplankton (phy), including proportions of terrestrial (OM_{terr}) and marine (OM_{mar}) sedimentary OM.

		P1		P2		P3		Avi.	Lag.	Rhi.	Phy.
		Wet	Dry	Wet	Dry	Wet	Dry				
TOC (%)	Min	0.5	1.0	2.8	2.3	2.4	2.2	42.1	37.9	41.3	10.3
	Max	1.8	1.9	3.8	2.9	3.0	2.8	44.2	45.1	44.9	11.0
	Mean	0.9	1.3	3.4	2.6	2.7	2.5	43.0	41.2	42.9	10.6
	SD	0.3	0.2	0.3	0.2	0.2	0.2	0.9	2.6	1.5	0.5
TN (%)	Min	0.04	0.08	0.20	0.19	0.20	0.19	1.2	1.3	1.3	1.7
	Max	0.15	0.17	0.27	0.24	0.23	0.26	1.6	1.9	1.5	1.8
	Mean	0.06	0.10	0.24	0.21	0.22	0.22	1.4	1.5	1.4	1.7
	SD	0.03	0.03	0.02	0.02	0.01	0.03	0.2	0.2	0.1	0.04
TP (%)	Min	0.009	0.018	0.036	0.028	0.036	0.033				
	Max	0.031	0.044	0.052	0.051	0.052	0.059				
	Mean	0.014	0.026	0.047	0.039	0.041	0.050				
	SD	0.005	0.007	0.004	0.008	0.005	0.009				
$\delta^{13}\text{C}$ (‰)	Min	-26.0	-25.7	-26.9	-26.4	-26.8	-25.8	-30.4	-30.4	-31.8	-24.4
	Max	-24.6	-24.2	-26.2	-24.7	-26.0	-24.2	-29.1	-28.2	-30.2	-23.4
	Mean	-25.3	-25.1	-26.6	-25.7	-26.3	-25.2	-29.4	-29.3	-30.8	-23.9
	SD	0.35	0.37	0.2	0.6	0.2	0.5	0.6	0.9	0.6	0.7
$\delta^{15}\text{N}$ (‰)	Min	5.2	4.4	5.3	5.1	6.1	5.9	5.0	2.6	1.7	3.2
	Max	8.4	7.2	7.2	6.4	7.3	7.2	6.4	5.3	4.6	3.7
	Mean	6.2	5.9	6.1	5.7	6.6	6.4	5.7	4.0	3.9	3.4
	SD	0.9	0.7	0.7	0.4	0.4	0.4	0.7	1.2	1.2	0.4
TOC/TN	Min	14.1	12.7	13.4	13.4	13.5	12.0	30.0	28.2	34.5	6.9
	Max	17.8	16.4	18.5	15.9	15.4	14.7	40.1	33.8	36.7	7.2
	Mean	16.2	14.5	16.5	14.8	14.1	13.3	35.0	31.4	35.6	7.1
	SD	0.9	1.1	1.2	0.7	0.4	0.8	4.3	2.3	0.8	0.2
TN/TP	Min	8.3	2.9	10.1	4.5	9.6	3.4				
	Max	11.7	8.1	12.5	11.8	13.7	9.7				
	Mean	9.7	4.3	11.4	5.9	12.0	4.8				
	SD	1.0	1.2	0.7	1.8	1.2	1.5				
OM_{terr} (%)	Min	12.6	5.7	38.1	13.8	35.1	4.8				
	Max	35.3	30.8	50.9	42.4	49.4	32.1				
	Mean	23.6	20.4	45.5	31.0	40.1	21.8				
	SD	6.0	6.2	3.4	9.5	3.9	8.7				
OM_{mar} (%)	Min	64.7	69.2	49.1	57.6	50.6	67.9				
	Max	87.4	94.3	61.9	86.2	64.9	95.2				
	Mean	76.4	79.6	54.5	69.0	59.9	78.2				
	SD	6.0	6.2	3.4	9.5	3.9	8.7				

Table 3
Component loadings of each variable obtained from PCA, variance explained and cumulative variance of the principal components (whole dataset).

Variables	PC1	PC2
Sand	-0.89	-0.02
Silt	0.88	0.01
Clay	0.84	0.14
TOC	0.92	-0.08
TN	0.93	-0.02
TP	0.80	0.05
$\delta^{13}\text{C}$	-0.57	0.19
$\delta^{15}\text{N}$	0.02	0.98
Eigen-values	4.89	1.02
% variance	61.67	12.87
% cumulative	61.67	74.54

Bold values represents the components which show significant positive loading.

4. Discussion

4.1. Sedimentary composition

The mudflat sediments were found to be mainly composed of a mixture containing silt and sand, reflecting a moderately high energetic environment, influenced by tide and fluvial process. The low hydrodynamic flow in the mangrove creeks (P2 and P3) likely caused an increase in the deposition of fine sediments. However, the MRE margin, where P1 was collected, appears to be more affected by tidal currents. In addition, the P1 site is located closer to the sand bar that likely contributed to the increase of fine sand in the sedimentary profile at this study site.

The spatial variations in the grain size distribution of the mudflat sediments play an important role in controlling the OM content. Silt and clay had positive strong to moderate correlation with TOC, TN and TP contents (r varied from 0.52 to 0.81). The first component of the PCA also indicated strong evidence that TOC, TN and TP increase as the silt and clay increase, with the highest TOC, TN and TP contents for P2 and P3 (Fig. 4a-b). Generally, fine-grained (silt + clay) sediments have higher %TOC than coarse sediments (Canfield, 1994), such relationships may be attributed to the fine-grained sediments which have large specific surface areas that provide higher capacity to adsorb OM (Loring and Rantala, 1992; Mayer, 1994).

The TOC and TN contents measured in the sediments during the

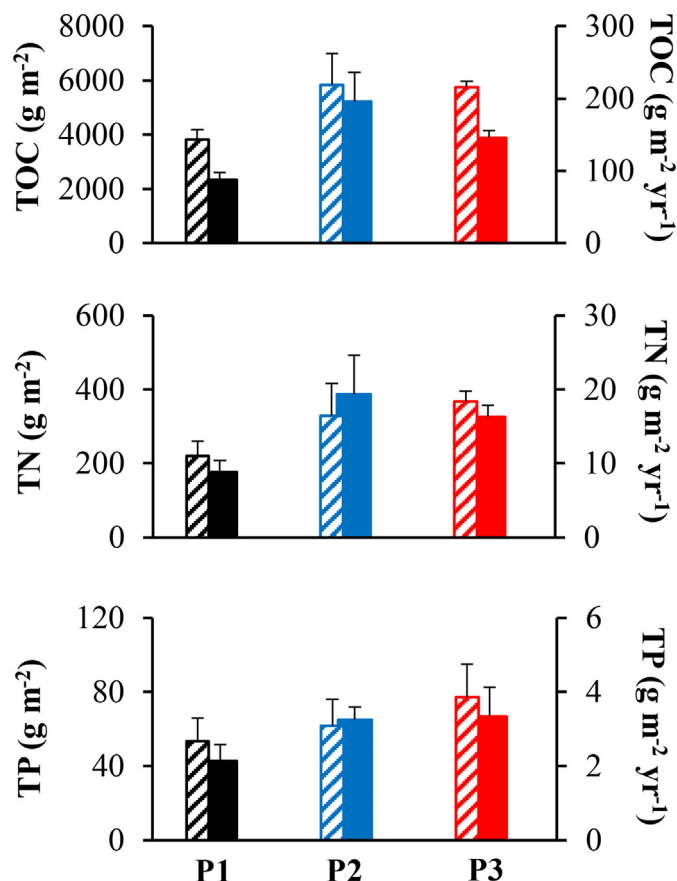


Fig. 5. TOC, TN and TP stocks (solid bars, g m^{-2}) and accumulation rates (striped bars, $\text{g m}^{-2} \text{ yr}^{-1}$) in the sediment cores (P1, P2 and P3). The error bars are based on the standard deviation from the average between the wet and dry season dataset.

present study are comparable to those reported in the adjacent coastal areas (Kauffman et al., 2018; Vilhena et al., 2018) and the TP contents are within the global average for mangrove (0.01–0.16%; Alongi et al., 1992). The gradual decrease of TOC, TN and TP content with depth in all cores likely reflect the decomposition of OM by microorganisms as

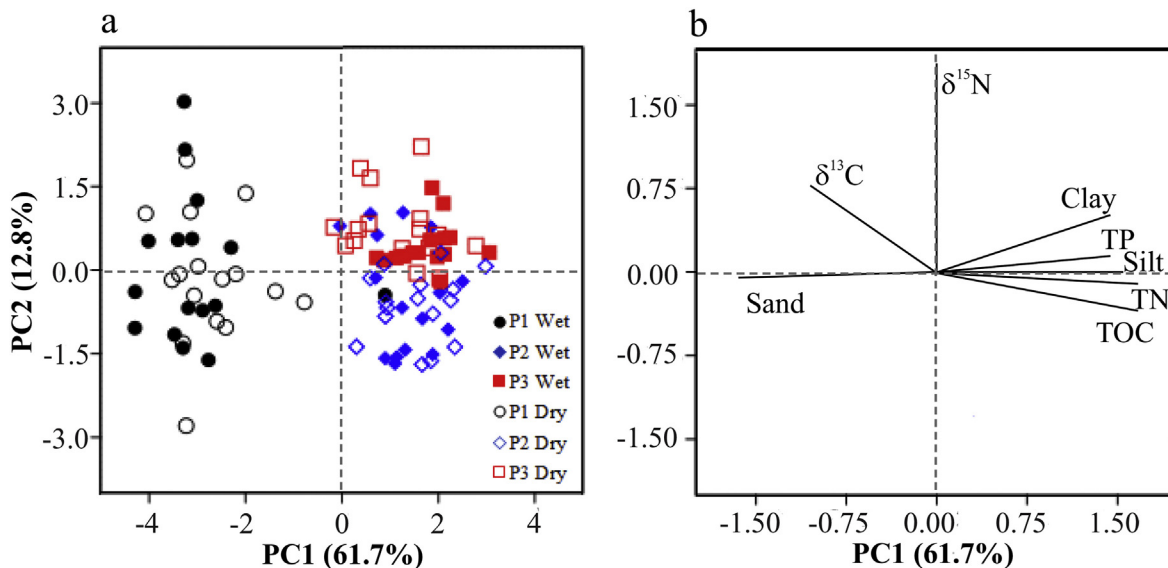


Fig. 4. (a) Principal Component Analysis (PCA) plot showing the multivariate variation among three sites in terms of environmental variables. (b) Vectors indicate the direction and strength of each environmental variable to the overall distribution. The first two principal axes explained 74.5% of the variance.

Table 4

The main variation and standard deviation (from each sediment core interval propagate to the average between the wet and dry season dataset) of total organic carbon, total nitrogen and total phosphorous stocks (g m^{-2}) and accumulation rates (AR) ($\text{g m}^{-2} \text{yr}^{-1}$) for the sediment cores (P1, P2 and P3).

Sites	TOC stock	TOC AR	TN stock	TN AR	TP stock	TP AR
P1	2337 \pm 279	143.2 \pm 26.3	177 \pm 31	11.0 \pm 2.4	43 \pm 9	2.7 \pm 0.7
P2	5218 \pm 1084	218.7 \pm 48.9	386 \pm 107	16.4 \pm 4.0	65 \pm 7	3.1 \pm 0.7
P3	3878 \pm 281	215.8 \pm 31.2	325 \pm 31	18.4 \pm 2.4	67 \pm 16	3.9 \pm 1.0
Overall average	3811 \pm 1389	192.5 \pm 50.6	296 \pm 109	15.3 \pm 4.3	58 \pm 15	3.2 \pm 1.0

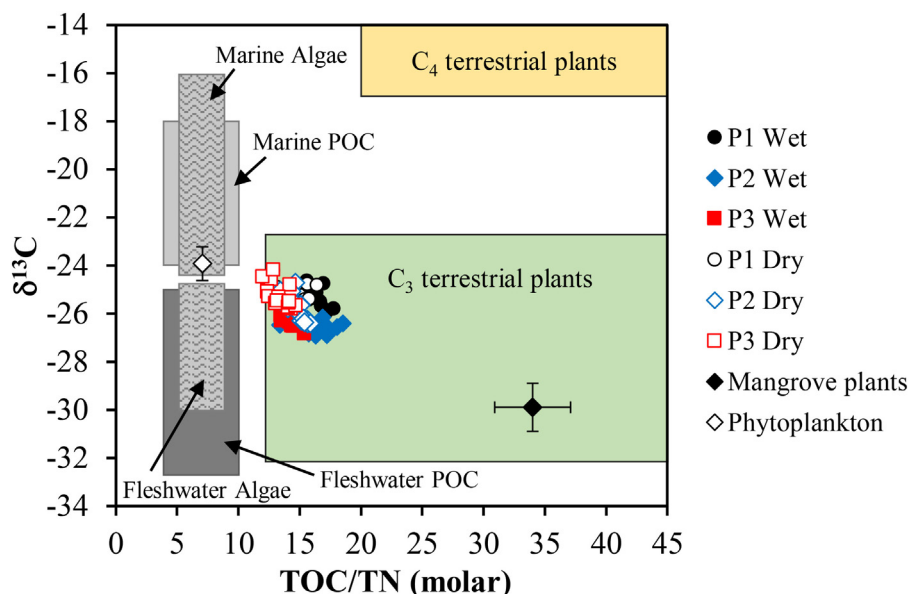


Fig. 6. Origin of sedimentary OM as indicated by $\delta^{13}\text{C}$ against TOC/TN (molar ratio). Fields are defined from the compilation of coastal sediments by Lamb et al. (2006). The phytoplankton (white diamond symbol) and Mangrove plants (black diamond symbol) endmember data are taken from the original data in this study.

noted in other systems (Kristensen et al., 2008) or a general increase in the OM content with time. The significant positive correlation between TOC and TN ($r = 0.96$) and TP ($r = 0.83$) in the sediments indicate that the nitrogen and phosphorous in the samples are predominantly associated with the organic fraction.

The TOC/TN/TP molar ratios in sediments were not significantly different in terms of spatial variability, but were significantly different seasonally: 171:11:1 in the wet season and 71:5:1 in the dry season. In both cases the TOC/TN/TP was different from the phytoplankton sources (Redfield: 106:16:1), with TN/TP ratios below 16 that suggest nitrogen to be the limiting factor for phytoplankton growth in these systems. This seasonal variation may be related to the diagenesis of OM. Higher TOC/TN molar ratios in wet than dry season indicate a greater contribution from OM of terrestrial origin, which is more refractory, during the wet season.

4.2. Sources of sedimentary organic matter

Different sources of OM often exhibit distinct elemental (carbon and nitrogen) and/or isotopic signatures ($\delta^{13}\text{C}$ and $\delta^{15}\text{N}$), representing useful indicators to quantify their relative contribution to the sedimentary OM. For example, C_3 plants are assumed to have TOC/TN > 12 (Meyers, 1997), $\delta^{13}\text{C}$ between -32‰ and -21‰ (Deines, 1980) and $\delta^{15}\text{N}$ around $0.4 \pm 0.9\text{‰}$ (Peterson and Howarth, 1987), while marine-derived OM is characterized by TOC/TN between 5 and 7 (Redfield et al., 1963), $\delta^{13}\text{C}$ from -16‰ to -23‰ (Meyers, 1994) and $\delta^{15}\text{N}$ around $8.6 \pm 1.0\text{‰}$ (Peterson and Howarth, 1987).

The potential sources to the sedimentary OM pool in mangrove-estuarine ecosystems can be upland forest and mangrove tissues (fresh leaf, stem, root, and litter), soils from river flow, aquatic macrophytes, microphytobenthos, and phytoplankton (Bouillon et al., 2008; Sasmito

et al., 2020). Some studies have also identified the presence of microphytobenthos as a potential source of OM in mudflats (Gontharet et al., 2014; Gorman et al., 2020), when microphytobenthos layers are visually detectable and thick enough to be sampled and separated from the sediments. However, the presence of microphytobenthos was not visually detectable in our sampling sites, therefore prohibiting the separation and analyses of a potential benthic microalgae endmember. Saltmarsh vegetation (*Spartina* spp.), dominated by C_4 plants, can be found at the mudflats along MRE. However, given that *Spartina* spp. and their sediments have enriched $\delta^{13}\text{C}$ signature, ranging from -14 to -12‰ and -18 to -14‰ , respectively (Currin et al., 1995; Kemp et al., 2010, and references therein), the depleted $\delta^{13}\text{C}$ values found in sediment samples suggests that *Spartina* spp. is not a major contributor of OM to the studied mudflat sediments. Therefore, we assumed mangrove plants and phytoplankton as the principal OM sources to the mudflats along MRE.

The $\delta^{13}\text{C}$ values of mangrove leaves (-31.8 to -28.2‰) are consistent with previously published results from other mangrove-estuarine ecosystems (Bouillon et al., 2008; Prasad and Ramanathan, 2009; Ranjan et al., 2011; Vilhena et al., 2018). The $\delta^{13}\text{C}$ and $\delta^{15}\text{N}$ values and TOC/TN molar ratio of phytoplankton (average of $-23.9 \pm 0.7\text{‰}$, $3.4 \pm 0.4\text{‰}$ and 7.1 ± 0.2 , respectively), which we extracted along the studied tidal creek, are close to the marine phytoplankton values. The $\delta^{13}\text{C}$ values are also similar to the reported value for marine DOC (average -23.7‰) extracted from Atlantic deep water in the adjacent study area (Dittmar et al., 2006).

The $\delta^{13}\text{C}$ (-26.9 to 24.2‰) versus TOC/TN (12.0 to 18.5) (Fig. 6) of the sedimentary OM suggests a mixture of sources contributing to the sedimentary OM pool, with a higher contribution of marine phytoplankton ($\delta^{13}\text{C}$: $-23.9 \pm 0.7\text{‰}$, TOC/TN: 7.1 ± 0.2) than mangrove-derived OM ($\delta^{13}\text{C}$: $-29.8 \pm 1.0\text{‰}$, TOC/TN: 34 ± 3.1). The $\delta^{15}\text{N}$

values of sediments (5.2–8.4‰, average of 6.2‰) are within a typical range of aquatic OM produced from assimilation of the nitrate pool. The slight increase of $\delta^{15}\text{N}$ values and TOC/TN molar ratios with depth, with exception to site P1 in the wet season, suggests anaerobic microbial degradation of OM in the deep reducing sediments (Meyers, 2003; Routh et al., 2009; Jennerjahn, 2012; Prasad et al., 2017). The peak of $\delta^{15}\text{N}$ at 14 cm in the site P1 during wet season could reflect an event provoked by input from a phytoplankton bloom or accumulation of allochthonous material deposited during and after a high rainfall event.

The consistently similar values of $\delta^{13}\text{C}$ throughout the sediment column suggest that the source of the depositional OM has been invariable during the past ~25 years at site P1. However, at sites P2 and P3, the enrichment of $\delta^{13}\text{C}$, during the dry season compared to wet season, indicated a shift in OM source, because the decomposition of OM usually does not cause a significant enrichment in $\delta^{13}\text{C}$ (Saintilan et al., 2013), and isotopic fractionation during the decomposition is typically < 3‰. This shift in OM accumulation source may be due to an increase in marine input in the upper layer (< 18 cm), likely associated with a larger sediment mixing provoked by bioturbation in the surface sediments, as the $\delta^{13}\text{C}$ values were relatively similar along the bottom layers.

The difference in OM source for terrestrial/mangrove C_3 plants ($\delta^{13}\text{C}$: $-29.8 \pm 1.0\text{‰}$) vs. marine phytoplankton ($\delta^{13}\text{C}$: $-23.9 \pm 0.7\text{‰}$) is distinct and hence, suitable for indicating the OM sources in the study area. However, $\delta^{15}\text{N}$ values and TOC/TN molar ratios can be unreliable because these may be influenced by diagenetic alterations (Prahl et al., 1997). Additionally, $\delta^{13}\text{C}$ did not show significant positive correlations with $\delta^{15}\text{N}$ ($r < 0.08$) and TOC/TN molar ratios ($r < 0.05$) in either the wet or dry season. Therefore, only $\delta^{13}\text{C}$ was used for the quantification analysis of OM. Based on the assumption of differing OM source input to the mudflat sediments, the end-member mixing model of terrestrial and marine OM showed that the contribution of OM sources varied between sites and seasons (Fig. 3, Table 1).

The OM_{mar} predominated in the studied sites likely due to the positioning of the sampling sites, which are situated near the mouth of the MRE (Atlantic Ocean). During the wet season (pore water salinity: 4–20), the OM_{mar} contribution was highest in the mudflat sediment from MRE margin (P1: 76.4%) compared to the mangrove tidal creeks (P2: 54.5, P3: 60%). During the dry season (pore water salinity: 18–25), due to less dilution from Marapanim River discharge, the influence of salt water is greater, thereby increasing the contribution of OM_{mar} by up to 18% (P1: 79.6, P2: 69 and P3: 78%). Overall, the downcore profiles of OM_{mar} and OM_{terr} remained relatively constant throughout the sediment columns during the wet season, but during the dry season an increase in marine input in the upper layers (< 18 cm) is noted at sites P2 and P3 (Fig. 3).

4.3. Carbon and nutrient accumulation rates and stocks

The TOC, TN and TP accumulation rates and stocks showed differences between the sites (Table 2, Fig. 5). The highest stocks and accumulation rates were found in the mudflat sediment from mangrove tidal creek (P2 and P3) compared to the MRE margin (P1). Two factors may cause these differences. Firstly, although site P1 presented the highest sedimentation rate (Fig. 2) and highest density (Fig. 3), it is composed of > 50% sand content with lower TOC, TN and TP contents compared to the sites P2 and P3. Previous studies indicated that OM preservation is often enhanced by the large surface area of fine-grained sediments, and the low energy associated with slack water deposits (Mayer, 1994; Keil et al., 1994). Sites P2 and P3 are protected from the direct impact of tidal energy and waves, as compared to site P1 that is located in the MRE margin and close to a sand bar.

The other factor is that the efficiency of OM storage in the mudflat sediments is also dependent on the origin of OM (Saintilan et al., 2013; Watanabe and Kuwae, 2015; Kusumaningtyasa et al., 2019). OM

proportions in our simple end-member mixing model indicated that 49–95% of OM contribution is from marine OM. The slight increase in fluxes of terrestrial OM along the mangrove tidal creek sites (P2 and P3, Table 1) contributed to higher TOC, TN and TP accumulation rates and stocks than those noted from the MRE margin (P1). These results were corroborated with previous studies, which indicated the terrestrial OM is preserved more efficiently than phytoplankton-derived OM in estuarine sediments (Hedges et al., 1997).

The average TOC accumulation rate (TOC AR) calculated in the studied mudflats was slightly higher ($192.5 \pm 43.5 \text{ g C m}^{-2} \text{ yr}^{-1}$) than the global average in conserved mangrove ($170 \text{ g C m}^{-2} \text{ yr}^{-1}$, Pérez et al., 2018) and the current global average for mangrove ecosystems ($179.6 \text{ g C m}^{-2} \text{ yr}^{-1}$, Alongi, 2020). Higher rates of $555 \text{ g C m}^{-2} \text{ yr}^{-1}$ were measured in other tropical mudflat in Piraquê-Açu estuary, Brazil, supported by high SAR (1.8 cm yr^{-1} , Bernardino et al., 2020). In contrast, lower carbon accumulation rates were reported in subtropical microtidal creeks systems. For example, Marchio et al. (2016) evidenced TOC AR of $162 \text{ g C m}^{-2} \text{ yr}^{-1}$ in Southwest Florida, and Santos et al. (2019) observed TOC AR of $63 \text{ g C m}^{-2} \text{ yr}^{-1}$ in a tidal creek in Evans Head, Australia. However, according Pérez et al. (2018), the distribution of TOC AR within the forests and adjacent sites (margin and mudflat environments) of mangrove ecosystems exhibited non-significant differences among regions, as variations are influenced by a combination of many local factors (e.g. geomorphology, vegetation cover, flooding frequency, hydrological regime and anthropogenic influence).

The average TN and TP accumulation rates were also high (TN: $15.3 \text{ g m}^{-2} \text{ yr}^{-1}$ and TP: $3.2 \text{ g m}^{-2} \text{ yr}^{-1}$; Table 4) when compared to the global average of anthropogenically non-impacted mangroves (TN: $8.9 \text{ g m}^{-2} \text{ yr}^{-1}$ and TP: $0.5 \text{ g m}^{-2} \text{ yr}^{-1}$, Breithaupt et al., 2014). Similar to our study, Bernardino et al. (2020) measured high TN accumulation rates of $27.9 \text{ g m}^{-2} \text{ yr}^{-1}$ in a conserved mudflat in Piraquê-Açu estuary. OM enriched in nutrients may be expected to decompose faster and to a larger extent than nutrient-depleted OM (Kristensen and Hansen, 1995; McGlathery et al., 2007). Thereby, the capacity to sequester OC may decrease with an increase in TN and TP burial rates (Breithaupt et al., 2014). However, in our study area TOC AR were higher in the sites with higher TN and TP AR. Similarly, TOC stocks were higher in the sites with higher TN and TP stocks (Table 4).

Due to the relatively shallow sediment depth (30 cm) used in our study, it is difficult to directly compare our results with those from other studies which usually assess sediment stocks based on deeper sediment profiles (e.g., $\geq 100 \text{ cm}$, Howard et al., 2014). However, we found some studies similar to ours with more superficial sampling. Our TOC stocks ranged from 2333 to 5218 g C m^{-2} (average of 3811 g C m^{-2}), which is similar those mudflat of West Papua, Indonesia (in the top 50 cm, 6200 g C m^{-2} ; Sasmito et al., 2020), Araçá Bay, Brazil (in the top 20 cm, range from 1700 to 2200 g C m^{-2} ; Gorman et al., 2020), and for unvegetated mudflats of China (in the top 50 cm, 4808 g C m^{-2} ; Feng et al., 2019). Comparing our stocks results with the values found in other Amazon mangroves sediments (in the top 30 cm) (supplementary information in Kauffman et al., 2018), our values are within the range of 3430–6230 g C m^{-2} , except at site P1 that was relatively lower ($2337 \pm 279 \text{ g C m}^{-2}$), which can be attributed to coarse textured sediments. These results suggest that mudflat along tidal creeks also have a high potential for organic carbon storage compared to vegetated habitats such as mangrove forests.

Few studies have assessed nitrogen and phosphorus stocks in mangrove and mudflat sediments. Feng et al. (2017) measured TN and TP stocks in an unvegetated mudflat of China (in the top 40 cm). Their average of TN stock of $\sim 290 \text{ g N m}^{-2}$ is comparable to $296 \pm 109 \text{ g N m}^{-2}$ (Table 4) in our study, but TP stock of $\sim 150 \text{ g P m}^{-2}$ is higher than what we found of $58 \pm 15 \text{ g P m}^{-2}$ (Table 4). Saderne et al., (2020) measured TN and TP stocks in mangrove sediments (in the top 20 cm) in the central Red Sea (99 g N m^{-2} and 70 g P m^{-2}) and along the Gulf coast of Saudi Arabia (223 g N m^{-2} and 32.8 g

P m^{-2}), where TN and TP stocks in the Gulf were quite comparable to what is presented here, but TN stocks were at least twofold higher in the Gulf compared to the Red Sea, while TP stocks were a maximum of 1.2 times higher in Red Sea. Pérez et al. (2017) observed in a conserved mangrove forest in New Zealand estuary TN stock between 400 and 500 g N m^{-2} , in the top 40 cm, which is slightly higher than our values. In contrast, Ray et al. (2014) and Ray et al. (2017) measured the TN and TP stocks, respectively, in the top 60 cm sediment in the Indian Sundarban mangrove and found an average of 4.2 g N m^{-2} and 0.4 g P m^{-2} , which are lower than what we found ($58 \pm 15 \text{ g P m}^{-2}$, Table 4), likely as a result of the TN and TP conserved in the living biomass.

The capacity to sequester and store OM in the studied creek mudflats likely reflects the SAR ($1.5 \pm 0.3 \text{ cm yr}^{-1}$), which is higher than the global average in conserved mangrove ($0.36 \pm \text{cm yr}^{-1}$; Pérez et al., 2018) and the current global average (0.77 cm yr^{-1} ; Breithaupt et al., 2012). This high SAR is supported by strong interaction between the river stream and the tides that characterize this environment, being close to the highest global accumulation rates in the mangrove forest (Breithaupt et al., 2012; Kusumaningtyasa et al., 2019) and mudflat (Bernardino et al., 2020). In general, the sedimentation rate is considered as a driving factor controlling the OM burial efficiency (Canfield, 1994). Although the sedimentary OM with a high proportion of marine origin tends to be more susceptible to decomposition, sites with high sedimentation rates contribute significantly to preserve OM (Hedges and Keil, 1995; Canfield et al., 2005). In addition, it should be noted that the studied mangrove area is densely inhabited by *Rhizophora*, *Avicennia* and *Laguncularia* trees, with heights up to 33 m. Therefore, these rates probably reflect a high productivity that provided a large supply of mangrove litter and dead roots to the mangrove creeks through tidal exchange.

Recently, Call et al. (2019) demonstrated that a mangrove tidal creek in Amazon presented large CO_2 and CH_4 fluxes from a nearby mangrove tidal creek. However, our results indicate that the Amazon mangrove creeks are also sites that accumulate considerable amounts of organic carbon (Fig. 7). For example, the total mudflat area in the tidal creek catchment of this study was near 0.5 km^2 (Fig. 1c), and

considering an average of the TOC accumulation rates between the three study sites, we estimate that a total of $96 \text{ kg TOC yr}^{-1}$ is sequestered in these creeks catchment. This suggests a previously unaccounted carbon sink in creek environments that are relevant to the carbon budgets along mangrove-colonized coastal zones. Therefore, mangrove tidal creeks can play an important role in the carbon cycling in tropical land-sea interfaces more than just acting as a conduit for exchanges between mangrove forests and coastal waters.

Considering global average in conserved mangrove of $170 \text{ g C m}^{-2} \text{ yr}^{-1}$ (Pérez et al., 2018) and the mangrove forest area within the catchment of this study was $7,638,368 \text{ m}^2$, we estimate that a total of $1299 \text{ t TOC yr}^{-1}$ is sequestered in these mangrove soils. Thus, the creek mudflat area accumulates around 0.007% of what would be estimated for the mangrove forest soils. Carbon dioxide emissions at the water-air interface were $2794 \pm 2072 \text{ g m}^{-2} \text{ yr}^{-1}$ ($174 \pm 129 \text{ mmol m}^{-2} \text{ d}^{-1}$) from a nearby mangrove tidal creek (Call et al., 2019). Using our creek mudflat area (0.5 km^2), CO_2 emissions would be $1397 \text{ kg C-CO}_2 \text{ yr}^{-1}$, while total mudflat sediment carbon burial would be 96.3 kg yr^{-1} . Therefore, sediment carbon sequestration in this system may offset < 7.0% of the aquatic CO_2 emissions.

5. Conclusion

This study investigated the recent (24 ± 4 years) carbon and nutrient accumulation rates and stocks in intertidal mudflats situated along mangrove creeks within the Brazilian Amazon coast. Even though marine OM was predominant along our study sites (49% to 95%), fine-grained sediments and higher terrestrial OM input, a product of a dense and tall mangroves trees, contributed to higher rates of TOC, TN, and TP accumulation and stocks in the mangrove tidal creeks (P2 and P3) compared to the Marapanim River estuary margin (P1). The capacity to sequester and store TOC also increased with increases in TN and TP burial rates and stocks. Due to the high sedimentation rates ($1.5 \pm 0.3 \text{ cm yr}^{-1}$), the TOC (192.5 ± 43.5), TN (15.3 ± 4.1), and TP (3.2 ± 0.8) accumulation rates found here were slightly higher than the global averages estimated for mangrove forest sediments. The potential of intertidal mudflats to sequester OC suggests that the creek

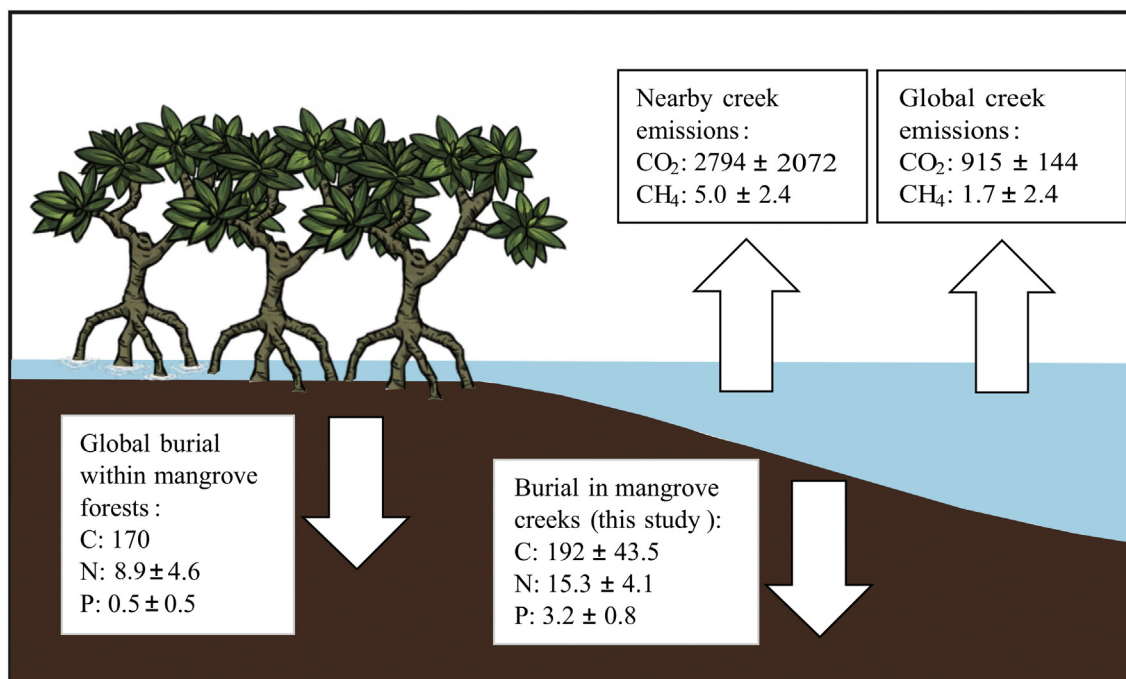


Fig. 7. Schematic comparing the global carbon (Pérez et al., 2018) and nitrogen and phosphorus burial rates (Breithaupt et al., 2014) for conserved mangrove forest with Marapanim mangrove creek (this study) and the global mangrove water-atmosphere CO_2 and CH_4 flux rates (Rosentretter et al., 2018) with “Furo do Meio” mangrove creek (Call et al., 2019). All rates are in $\text{g m}^{-2} \text{ yr}^{-1}$.

environments are unaccounted carbon sinks and are relevant in terms of carbon budgets in mangrove-colonized coastal zones.

Declaration of Competing Interest

The authors declare that they have no known competing financial interests or personal relationships that could have appeared to influence the work reported in this paper.

Acknowledgements

The authors thank the research grants from the Brazilian Ministry of Education (CAPES) and Brazilian Research Council (CNPq) to C.R.L. Matos and W. Machado. C.J. Sanders is supported by Australian Research Council (DE160100443) and E. Metzger by CNRS-EC2CO project Vubleu.

Appendix A. Supplementary data

Supplementary data to this article can be found online at <https://doi.org/10.1016/j.margeo.2020.106317>.

References

- AgisoftPhotoScan, 2018. Agisoft PhotoScan Professional. Version 1.4.5. Agisoft LLC, St. Petersburg, Russia Retrieved from. <http://www.agisoft.com/downloads/installer/>.
- Alongi, D.M., 2014. Carbon cycling and storage in mangrove forests. *Annu. Rev. Mar. Sci.* 6, 195–219. <https://doi.org/10.1146/annurev-marine-010213-135020>.
- Alongi, D.M., 2020. Global significance of mangrove blue carbon in climate change mitigation (Version 1). *Sci* 2, 57.
- Alongi, D.M., Boto, K.G., Robertson, A.I., 1992. Nitrogen and phosphorus cycles. In: Robertson, A.I., Alongi, D.M. (Eds.), *Tropical Mangrove Ecosystems. Coastal and Estuarine Studies*. American Geophysical Union, Washington, DC, pp. 251–292. <https://doi.org/10.1029/ce041p0251>.
- Appleby, P.G., Oldfield, F., 1992. Application of lead-210 to sedimentation studies. In: Ivanovich, M., Harmon, S. (Eds.), *Uranium Series Disequilibrium: Application to Earth, Marine and Environmental Science*, second ed. Oxford Science Publications, pp. 731–783.
- Arias-Ortiz, A., Masqué, P., Garcia-Orellana, J., Serrano, O., Mazarrasa, I., Marbà, N., Lovelock, C.E., Lavery, P.S., Duarte, C.M., 2018. Reviews and syntheses: ²¹⁰Pb-derived sediment and carbon accumulation rates in vegetated coastal ecosystems – setting the record straight. *Biogeosciences* 15, 6791–6818. <https://doi.org/10.5194/bg-15-6791-2018>.
- Aspila, K.L., Agemian, H., Chau, A.S.Y., 1976. A semi-automated method for the determination of inorganic, organic and total phosphate in sediments. *Analyst* 101, 187–197. <https://doi.org/10.1039/AN9760100187>.
- Bernardino, A.F., Sanders, C.J., Bissoli, L.B., de Gomes, L.E., Kauffman, J.B., Ferreira, T.O., 2020. Land use impacts on benthic bioturbation potential and carbon burial in Brazilian mangrove ecosystems. *Limnol. Oceanogr.* 9999, 1–11. <https://doi.org/10.1002/lno.11458>.
- Berrêdo, J.F., Costa, M.L., Progene, M.P.S., 2008. Efeitos das variações sazonais do clima tropical úmido sobre as águas e sedimentos de manguezais do estuário do rio Marapanim, costa nordeste do Estado do Pará. *Acta Amazon.* 38, 473–482. <https://doi.org/10.1590/S0044-59672008000300012>.
- Blott, S.J., Pye, K., 2001. GRADISTAT: a grain size distribution and statistics package for the analysis of unconsolidated sediments. *Earth Surf. Process. Landf.* 26, 1237–1248. <https://doi.org/10.1002/esp.261>.
- Bouillon, S., Connolly, R.M., Lee, S.Y., 2008. Organic matter exchange and cycling in mangrove ecosystems: recent insights from stable isotope studies. *J. Sea Res.* 59, 44–58. <https://doi.org/10.1016/j.seares.2007.05.001>.
- Breithaupt, J.L., Smoak, J.M., Smith, T.J., Sanders, C.J., Hoare, A., 2012. Organic carbon burial rates in mangrove sediments: strengthening the global budget. *Glob. Biogeochem. Cycles* 26. <https://doi.org/10.1029/2012gb004375>.
- Breithaupt, J.L., Smoak, J.M., Smith, T.J., Sanders, C.J., 2014. Temporal variability of carbon and nutrient burial, sediment accretion, and mass accumulation over the past century in a carbonate platform mangrove forest of the Florida Everglades. *J. Geophys. Res. Biogeosci.* 119, 2032–2048. <https://doi.org/10.1002/2014JG002715>.
- Call, M., Santos, I.R., Dittmar, T., Rezende, C.E., Asp, N.E., Maher, D.T., 2019. High pore-water derived CO₂ and CH₄ emissions from a macro-tidal mangrove creek in the Amazon region. *Geochim. Cosmochim. Acta* 247, 106–120. <https://doi.org/10.1016/j.gca.2018.12.029>.
- Canfield, D.E., 1994. Factors influencing organic carbon preservation in marine sediments. *Chem. Geol.* 114, 315–329. [https://doi.org/10.1016/0009-2541\(94\)90061-2](https://doi.org/10.1016/0009-2541(94)90061-2).
- Canfield, D.E., Kristensen, E., Thamdrup, B., 2005. Heterotrophic carbon metabolism. *Aquat. Geomicrobiol. Adv. Mar. Biol.* 48, 129–166. [https://doi.org/10.1016/S0065-2881\(05\)48005-0](https://doi.org/10.1016/S0065-2881(05)48005-0).
- Carvalho, M.C., Eickhoff, W., Drexler, M., 2020. Open-source autosampler for elemental and isotopic analyses of solids. *HardwareX* 8 (e00123), 1–22. <https://doi.org/10.1016/j.ohx.2020.e00123>.
- Chambers, L.G., Davis, S.E., Troxler, T., Boyer, J.N., Downey-Wall, A., Scinto, L.J., 2013. Biogeochemical effects of simulated sea level rise on carbon loss in an Everglades mangrove peat soil. *Hydrobiologia* 726, 195–221. <https://doi.org/10.1007/s10750-013-1764-6>.
- Cohen, M.C.L., de Souza, A.V., Rossetti, D.F., Pessenda, L.C.R., França, M.C., 2018. Decadal-scale dynamics of an Amazonian mangrove caused by climate and sea level changes: inferences from spatial-temporal analysis and Digital Elevation Models. *Earth Surf. Process. Landf.* 43, 2876–2888. <https://doi.org/10.1002/esp.4440>.
- Cohen, M.C.L., Figueiredo, B.L., Oliveira, N.N., Fontes, N.A., França, M.C., Pessenda, L.C.R., Lima, P., 2019. Impacts of Holocene and modern sea-level changes on estuarine mangroves from Northeastern Brazil. *Earth Surf. Process. Landf.* <https://doi.org/10.1002/esp.4737>.
- Curran, C.A., Newell, S.Y., Paerl, H.W., 1995. The Role of Standing Dead *Spartina* Alterniflora and Benthic Microalgae in Salt Marsh Food Webs: Considerations Based on Multiple Stable Isotope Analysis. *Mar. Ecol. Prog. Ser.* 121, 99–116.
- Darrow, E.S., Carmichael, R.H., Calci, K.R., Burkhardt, W., 2017. Land-use related changes to sedimentary organic matter in tidal creeks of the northern Gulf of Mexico. *Limnol. Oceanogr.* 62, 686–705. <https://doi.org/10.1002/lno.10453>.
- Deines, P., 1980. The isotopic composition of reduced organic carbon. In: Fritz, P., Fontes, J.C. (Eds.), *Handbook of Environmental Isotope Geochemistry. The Terrestrial Environment*. vol. 1. A. Elsevier, Amsterdam, pp. 329–406. <https://doi.org/10.1016/B978-0-444-41780-0.50015-8>.
- Dittmar, T., Hertkorn, N., Kattner, G., Lara, R.J., 2006. Mangroves, a major source of dissolved matter sources to the oceans. *Glob. Biogeochem. Cycles* 20, GB1012. <https://doi.org/10.1029/2005GB002570>.
- Feng, J., Zhou, J., Wang, L., Cui, X., Ning, C., Wu, H., Zhu, X., Lin, G., 2017. Effects of short-term invasion of *Spartina alterniflora* and the subsequent restoration of native mangroves on the soil organic carbon, nitrogen and phosphorus stock. *Chemosphere* 184, 774–783. <https://doi.org/10.1016/j.chemosphere.2017.06.060>.
- Feng, J., Wang, S., Wang, S., Ying, R., Yin, F., Jiang, L., Li, Z., 2019. Effects of invasive *Spartina alterniflora* Loisel. and subsequent ecological replacement by *Sonneratia apetala* Buch.-Ham. on soil organic carbon fractions and stock. *Forests* 10, 171. <https://doi.org/10.3390/f10020171>.
- Fernandes, M.E.B., Oliveira, F.P., Eyzaguirre, I.A.L., 2018. Mangroves on the Brazilian Amazon coast: Uses and rehabilitation. In: Makowski, C., Finkl, C. (Eds.), *Threats to Mangrove Forests*. Coastal Research Library. vol 25 Springer, Cham. https://doi.org/10.1007/978-3-319-73016-5_29.
- Giri, C., Ochieng, E., Tieszen, L.L., Zhu, Z., Singh, A., Loveland, T., Masek, J., Duke, N., 2011. Status and distribution of mangrove forests of the world using earth observation satellite data. *Glob. Ecol. Biogeogr.* 20, 154–159. <https://doi.org/10.1111/j.1466-8238.2010.00584.x>.
- GlobalMapper, 2017. (Version 19). Blue Marble Geographics. Hallowell, Maine, United State.
- Gontharet, S., Mathieu, O., Lévêque, J., Milloux, M.-J., Lesourd, S., Philippe, S., Caillaud, J., Gardel, A., Sarrazin, M., Proisy, C., 2014. Distribution and sources of bulk organic matter (OM) on a tropical intertidal mud bank in French Guiana from elemental and isotopic proxies. *Chem. Geol.* 376, 1–10. <https://doi.org/10.1016/j.chemgeo.2014.03.009>.
- Gorman, D., Sumida, P.Y.G., Figueira, R.C.L., Turra, A., 2020. Improving soil carbon estimates of mudflats in Aracá Bay using spatial models that consider riverine input, wave exposure and biogeochemistry. *Estuar. Coast. Shelf Sci.* 238, 106734. <https://doi.org/10.1016/j.ecss.2020.106734>.
- Grasshoff, K., Kremling, K., Ehrhardt, M., 1999. *Methods of Seawater Analysis*, third ed. Wiley, New York. <https://doi.org/10.1002/9783527613984>.
- Hammer, O., Harper, D.A.T., Ryan, P.D., 2001. PAST: paleontological statistics software package for education and data analysis. *Palaentol. Electron.* 4 (1) (9 pp). https://palaeo-electronica.org/2001_1/past/issue1_01.htm.
- Hedges, J.I., Keil, R.G., 1995. Sedimentary organic matter preservation: an assessment and speculative synthesis. *Mar. Chem.* 49, 81–115. [https://doi.org/10.1016/0304-4203\(95\)00008-F](https://doi.org/10.1016/0304-4203(95)00008-F).
- Hedges, J.I., Keil, R.G., Benner, R., 1997. What happens to terrestrial organic matter in the ocean? *Org. Geochem.* 27, 195–212. [https://doi.org/10.1016/S0146-6380\(97\)00066-1](https://doi.org/10.1016/S0146-6380(97)00066-1).
- Howard, J., Hoyt, S., Isensee, K., Pidgeon, E., Telszewski, M., 2014. Coastal Blue Carbon: Methods for Assessing Carbon Stocks and Emissions Factors in Mangroves, Tidal Salt Marshes, and Seagrass Meadows. *Conserv. Int. Intergov. Oceanogr. Comm. UNESCO, Int. Union Conserv. Nature, Arlington, Virginia, USA*. pp. 1–180.
- ICMBio, 2018. *Atlas dos Manguezais do Brasil*, 1st ed. Instituto Chico Mendes de Conservação da Biodiversidade, Brasília. [https://doi.org/10.1016/S0146-6380\(97\)00066-1](https://doi.org/10.1016/S0146-6380(97)00066-1). (176 p).
- Jennerjahn, T.C., 2012. Biogeochemical response of tropical coastal systems to present and past environmental change. *Earth Sci. Rev.* 114, 19–41. <https://doi.org/10.1016/j.earscirev.2012.04.005>.
- Jennerjahn, T.C., Ittekkot, V., 2002. Relevance of mangroves for the production and deposition of organic matter along tropical continental margins. *Naturwissenschaften* 89 (1), 23–30. <https://doi.org/10.1007/s00114-001-0283-x>.
- Kauffman, J.B., Bernardino, A.F., Ferreira, T.O., Giovannoni, L.R., de Gomes, L.E., Romero, D.J., Jimenez, L.C.Z., Ruiz, F., 2018. Carbon stocks of mangroves and salt marshes of the Amazon region, Brazil. *Biol. Lett.* 14, 20180208. <https://doi.org/10.1098/rsbl.2018.0208>.
- Keil, R.G., Montluçon, D.B., Prah, F.G., Hedges, J.I., 1994. Sorptive preservation of labile organic matter in marine sediments. *Nature* 370, 549–552.
- Kemp, A.C., Vane, C.H., Horton, B.P., Culver, S.J., 2010. Stable carbon isotopes as potential sea-level indicators in salt marshes, North Carolina, USA. *The Holocene* 20 (4), 623–636. <https://doi.org/10.1177/0959683609354302>.

- Kjerve, B., Lacerda, L.D., 1993. Mangroves of Brazil. In: *Conservation and Sustainable Utilization of Mangrove Forests in Latin America and Africa Regions. Part 1: Latin America*. ITTO/ISME Project PD114/90(F), pp. 245–272.
- Kristensen, E., Hansen, K., 1995. Decay of plant detritus in organic-poor marine sediment: production rates and stoichiometry of dissolved C and N compounds. *J. Mar. Res.* 53, 675–702. <https://doi.org/10.1357/0022240953213115>.
- Kristensen, E., Bouillon, S., Dittmar, T., Marchand, C., 2008. Organic carbon dynamics in mangrove ecosystems: a review. *Aquat. Bot.* 89 (2), 201–219. <https://doi.org/10.1016/j.aquabot.2007.12.005>.
- Kusumaningtyasa, M.A., Hutahaean, A.A., Fischer, H.W., Mayod, M.P., Ransbyd, D., Jennerjahn, T.C., 2019. Variability in the organic carbon stocks, sources, and accumulation rates of Indonesian mangrove ecosystems. *Estuar. Coast. Shelf Sci.* 218, 310–323. <https://doi.org/10.1016/j.eccs.2018.12.007>.
- Lamb, A.L., Wilson, G.P., Leng, M.J., 2006. A review of coastal palaeoclimate and relative sea-level reconstructions using $\delta^{13}\text{C}$ and C/N ratios in organic material. *Earth-Sci. Rev.* 75, 29–57. <https://doi.org/10.1016/j.earscirev.2005.10.003>.
- Liu, D., Li, X., Emeis, K.C., Wang, Y., Richard, P., 2015. Distribution and sources of organic matter in surface sediments of Bohai Sea near the Yellow River Estuary, China. *Estuar. Coast. Shelf Sci.* 165, 128–136. <https://doi.org/10.1016/j.eccs.2015.09.007>.
- Loring, D.H., Rantala, R.T.T., 1992. Manual for the geochemical analyses of marine sediments and suspended particulate matter. *Earth-Sci. Rev.* 32, 235–283. [https://doi.org/10.1016/0012-8252\(92\)90001-A](https://doi.org/10.1016/0012-8252(92)90001-A).
- Marchio, D., Savarese, M., Bovard, B., Mitsch, W., 2016. Carbon sequestration and sedimentation in mangrove swamps influenced by hydrogeomorphic conditions and urbanization in Southwest Florida. *Forests* 7 (12), 116. <https://doi.org/10.3390/f7060116>.
- Martorano, L.G., Pereira, L.C., Cesar, E.G.M., Pereira, I.C.B., 1993. *Estudos Climáticos do Estado do Pará, Classificação Climática (Köppen) e Deficiência Hídrica (Thorntonwhite, Mather)*. Belém, SUDAM/EMBRAPA, SNLCS, pp. 53.
- Mayer, L.M., 1994. Surface area control of organic carbon accumulation in continental shelf sediments. *Geochim. Cosmochim. Acta* 58, 1271–1284. [https://doi.org/10.1016/0016-7037\(94\)90381-6](https://doi.org/10.1016/0016-7037(94)90381-6).
- McGlathery, K.J., Sundback, K., Anderson, I.C., 2007. Eutrophication in shallow coastal bays and lagoons: the role of plants in the coastal filter. *Mar. Ecol. Prog. Ser.* 348, 1–18. <https://doi.org/10.3354/meps07132>.
- McLeod, E., Chmura, G.L., Bouillon, S., Salm, R., Björk, M., Duarte, C.M., Lovelock, C.E., Schlesinger, W.H., Silliman, B.R., 2011. A blueprint for blue carbon: toward an improved understanding of the role of vegetated coastal habitats in sequestering CO_2 . *Front. Ecol. Environ.* 9, 552–560. <https://doi.org/10.1890/110004>.
- Meyers, P.A., 1994. Preservation of elemental and isotopic source identification of sedimentary organic matter. *Chem. Geol.* 114, 289–302. [https://doi.org/10.1016/0009-2541\(94\)90059-0](https://doi.org/10.1016/0009-2541(94)90059-0).
- Meyers, P.A., 1997. Organic geochemical proxies of paleoceanographic, paleolimnologic, and paleoclimatic processes. *Org. Geochem.* 27, 213–250. [https://doi.org/10.1016/S0146-6380\(97\)00049-1](https://doi.org/10.1016/S0146-6380(97)00049-1).
- Meyers, P.A., 2003. Applications of organic geochemistry to paleolimnological reconstructions: a summary of examples from the Laurentian Great Lakes. *Org. Geochem.* 34, 261–289. [https://doi.org/10.1016/S0146-6380\(02\)00168-7](https://doi.org/10.1016/S0146-6380(02)00168-7).
- Nascimento, W.R., Souza-Filho, P.W.M., Proisy, C., Lucas, R.M., Rosenqvist, A., 2013. Mapping changes in the largest continuous Amazonian mangrove belt using object-based classification of multisensor satellite imagery. *Estuar. Coast. Shelf Sci.* 117, 83–93. <https://doi.org/10.1016/j.eccs.2012.10.005>.
- Nellemann, C., Corcoran, E., Duarte, C.M., Valdres, L., Young, C.D., Fonseca, L., Grimsditch, G., 2009. *Blue Carbon - The Role of Healthy Oceans in Binding Carbon*. UN Environment, GRID-Arendal (ISBN: 978-82-7701-060-1).
- Paiva, R.S., Eskinazi-Leça, E., Passavante, J.Z.O., Silva-Cunha, M.G.G., Melo, N.F.A.C., 2006. Ecological considerations on phytoplankton from the Guajará bay and from the Guamá river estuary in Para, Brazil. *Bol. Mus. Para. Emílio Goeldi. Ciências Naturais* 1, 133–146.
- Pérez, A., Machado, W., Gutierrez, D., Stokes, D., Sanders, L., Smoak, J.M., Santos, I., Sanders, C.J., 2017. Changes in organic carbon accumulation driven by mangrove expansion and deforestation in a New Zealand estuary. *Estuar. Coast. Shelf Sci.* 192, 108–116. <https://doi.org/10.1016/j.eccs.2017.05.009>.
- Pérez, A., Libardoni, B.G., Sanders, C.J., 2018. Factors influencing organic carbon accumulation in mangrove ecosystems. *Biol. Lett.* 14 (10). <https://doi.org/10.1098/rsbl.2018.0237>.
- Peterson, B.J., Howarth, R.W., 1987. Sulfur, carbon, and nitrogen isotopes used to trace organic matter flow in the salt-marsh estuaries of Sapelo Island, Georgia. *Limnol. Oceanogr.* 32 (6), 1195–1213. <https://doi.org/10.4319/lo.1987.32.6.1195>.
- Prahl, F.G., De Lange, G.T., Scholten, S., Cowie, G.L., 1997. A case of post-depositional aerobic degradation of terrestrial organic matter in turbidite deposits from the Madeira Abyssal Plain. *Org. Geochem.* 27, 141–152. [https://doi.org/10.1016/S0146-6380\(97\)00078-8](https://doi.org/10.1016/S0146-6380(97)00078-8).
- Prasad, M.B.K., Ramanathan, A.L., 2009. Organic matter characterization in a tropical estuarine-mangrove ecosystem of India: preliminary assessment by using stable isotopes and lignin phenols. *Estuar. Coast. Shelf Sci.* 84 (4), 617–624. <https://doi.org/10.1016/j.eccs.2009.07.029>.
- Prasad, M.B.K., Kumar, A., Ramanathan, A.L., Datta, D.K., 2017. Sources and dynamics of sedimentary organic matter in Sundarban mangrove estuary from Indo-Gangetic delta. *Ecol. Process.* 6, 8. <https://doi.org/10.1186/s13717-017-0076-6>.
- Ranjan, R.K., Routh, J., Ramanathan, A.L., Klump, J.V., 2011. Elemental and stable isotope records of organic matter input and its fate in the Pichavaram mangrove-estuarine sediments (Tamil Nadu, India). *Mar. Chem.* 126, 163–172. <https://doi.org/10.1016/j.marchem.2011.05.005>.
- Ray, R., Majumder, N., Das, S., Chowdhury, C., Jana, T.K., 2014. Biogeochemical cycle of nitrogen in a tropical mangrove ecosystem, east coast of India. *Mar. Chem.* 167, 33–43. <https://doi.org/10.1016/j.marchem.2014.04.007>.
- Ray, R., Majumder, N., Chowdhury, C., Das, S., Jana, T.K., 2017. Phosphorus budget of the Sundarban mangrove ecosystem: box model approach. *Estuar. Coasts* 41, 1036–1049. <https://doi.org/10.1007/s12237-017-0332-0>.
- Redfield, A.C., Ketchum, B.H., Richards, F.A., 1963. The influence of organisms on the composition of sea-water. In: Hill, M.N. (Ed.), *The Composition of Seawater: Comparative and Descriptive Oceanography. The Sea: Ideas and Observations on Progress in the Study of the Seas*. 2, pp. 26–77.
- Rosentreter, J.A., Maher, D.T., Erler, D.V., Murray, R., Eyre, B.D., 2018. Seasonal and temporal CO_2 dynamics in three tropical mangrove creeks – a revision of global mangrove CO_2 emissions. *Geochim. Cosmochim. Acta* 222, 729–745. <https://doi.org/10.1016/j.gca.2017.11.026>.
- Routh, J., Meyers, P.A., Choudhury, P., Kumar, B., 2009. A sediment record of recent nutrient loading and trophic state change in Lake Norrviken, Sweden. *J. Paleolimnol.* 42, 325–341. <https://doi.org/10.1007/s10933-008-9279-2>.
- Saderne, V., Cusack, M., Serrano, O., Almahasheer, H., Krishnakumar, P.K., Rabaoui, L., Qurban, M.A., Duarte, C.M., 2020. Role of vegetated coastal ecosystems as nitrogen and phosphorus filters and sinks in the coasts of Saudi Arabia. *Environ. Res. Lett.* 15, 034058. <https://doi.org/10.1088/1748-9326/ab76da>.
- Saintilan, N., Rogers, K., Mazumder, D., Woodroffe, C., 2013. Allochthonous and autochthonous contributions to carbon accumulation and carbon store in southeastern Australian coastal wetlands. *Estuar. Coast. Shelf Sci.* 128, 84–92. <https://doi.org/10.1016/j.eccs.2013.05.010>.
- Sanders, C.J., Santos, I.R., Maher, D.T., Breithaupt, J.L., Smoak, J.M., Ketterer, M., Call, M., Sanders, L.M., Eyre, B.D., 2016. Examining $^{239+240}\text{Pu}$, ^{210}Pb and historical events to determine carbon, nitrogen and phosphorus accumulation in mangrove sediments of Moreton Bay, Australia. *J. Environ. Radioact.* 151, 623–629. <https://doi.org/10.1016/j.jenvrad.2015.04.018>.
- Santos, I.R., Maher, D.T., Larkin, R., Webb, J.R., Sanders, C.J., 2019. Carbon outwelling and outgassing vs. burial in an estuarine tidal creek surrounded by mangrove and saltmarsh wetlands. *Limnol. Oceanogr.* 64, 996–1013. <https://doi.org/10.1002/lno.11090>.
- Sasmito, D., Kuzyakov, Y., Lubis, A.A., Murdiyasar, D., Hutley, L.B., Bachri, S., Friess, D.A., Martius, C., Borchard, N., 2020. Organic carbon burial and sources in soils of coastal mudflat and mangrove ecosystems. *Catena* 187, 104414. <https://doi.org/10.1016/j.catena.2019.104414>.
- Schultz, D.J., Calder, J.A., 1976. Organic carbon $^{13}\text{C}/^{12}\text{C}$ variations in estuarine sediments. *Geochim. Cosmochim. Acta* 40, 381–385. [https://doi.org/10.1016/0016-7037\(76\)90002-8](https://doi.org/10.1016/0016-7037(76)90002-8).
- Seeberg-Elverfeldt, J., Schlüter, M., Feseker, T., Kölling, M., 2005. Rhizon sampling of pore waters near the sediment–water interface of aquatic systems. *Limnol. Oceanogr. Methods* 3, 361–371. <https://doi.org/10.4319/lom.2005.3.361>.
- Silva, C.A., Souza-Filho, P.W.M., Rodrigues, S.W.P., 2009. Morphology and modern sedimentary deposits of the macrotidal Marapanim Estuary (Amazon, Brazil). *Cont. Shelf Res.* 29, 619–631. <https://doi.org/10.1016/j.csr.2008.09.018>.
- Smoak, J.M., Breithaupt, J.L., Smith, T.J., Sanders, C.J., 2013. Sediment accretion and organic carbon burial relative to sea-level rise and storm events in two mangrove forests in Everglades National Park. *Catena* 104, 58–66.
- Steinmuller, H.E., Foster, T.E., Boudreau, P., Ross Hinkle, C., Chambers, L.G., 2020. Tipping points in the mangrove March: characterization of biogeochemical cycling along the mangrove–salt marsh ecotone. *Ecosystems* 23, 417–434. <https://doi.org/10.1007/s10021-019-00411-8>.
- Udden, J.A., 1914. Mechanical composition of clastic sediments. *Bull. Geol. Soc. Am.* 25, 655–744.
- Vilhena, M.P.S.P., Costa, M.L., Berrêdo, J.F., 2013. Accumulation and transfer of Hg, As, Se, and other metals in the sediment-vegetation-crab-human food chain in the coastal zone of the northern Brazilian state of Para (Amazonia). *Environ. Geochem. Health* 35, 477–494. <https://doi.org/10.1007/s10653-013-9509-z>.
- Vilhena, M.P.S.P., Costa, M.L., Berrêdo, J.F., Paiva, R.S., Moreira, M.Z., 2018. The sources and accumulation of sedimentary organic matter in two estuaries in the Brazilian Northern coast. *Reg. Stud. Mar. Sci.* 18, 188–196. <https://doi.org/10.1016/j.rmsa.2017.10.007>.
- Wang, F., Lu, X., Sanders, C.J., Tang, J., 2019. Tidal wetland resilience to sea level rise increases their carbon sequestration capacity in United States. *Nat. Commun.* 10 (5434), 1–11. <https://doi.org/10.1038/s41467-019-13294-z>.
- Watanabe, K., Kuwae, T., 2015. How organic carbon derived from multiple sources contributes to carbon sequestration processes in a shallow coastal system? *Glob. Chang. Biol.* 21, 2612–2623. <https://doi.org/10.1111/gcb.12924>.
- Wentworth, C.K., 1922. A scale of grade and class terms for clastic sediments. *J. Geol.* 30, 377–392.
- Zonneveld, K.A.F., Versteegh, G.J.M., Kasten, S., Eglinton, T.I., Emeis, K.-C., Huguet, C., Koch, B.P., de Lange, G.J., de Leeuw, J.W., Middelburg, J.J., Mollenhauer, G., Prahl, F., Rethemeyer, J., Wakeham, S., 2010. Selective preservation of organic matter in marine environments: processes and impact on the fossil record. *Biogeosciences* 7, 483–511. <https://doi.org/10.5194/bg-7-483-2010>.